Hisashi Hayakawa, Denny M Oliveira, Margaret A Shea, Don F Smart, Seán P Blake, Kentaro Hattori, Ankush T Bhaskar, Juan J Curto, Daniel R Franco, Yusuke Ebihara, The Extreme Solar and Geomagnetic Storms on 20-25 March 1940, Monthly Notices of the Royal Astronomical Society, 2021;, stab3615, https://doi.org/10.1093/mnras/stab3615

The Extreme Solar and Geomagnetic Storms on 20-25 March 1940

Hisashi Hayakawa (1 – 4)*, Denny M. Oliveira (5 – 6), Margaret A. Shea (7), Don F. Smart (7), Seán P. Blake (5, 8), Kentaro Hattori (9), Ankush T. Bhaskar (10), Juan J. Curto (11), Daniel R. Franco (12), Yusuke Ebihara (13)

(1) Institute for Space-Earth Environmental Research, Nagoya University, Nagoya, 4648601, Japan (2) Institute for Advanced Research, Nagoya University, Nagoya, 4648601, Japan
(3) UK Solar System Data Centre, Space Physics and Operations Division, RAL Space, Science and Technology Facilities Council, Rutherford Appleton Laboratory, Harwell Oxford, Didcot, Oxfordshire, OX11 0QX, UK
(4) Nishina Centre, Riken, Wako, 3510198, Japan
(5) Heliophysics Science Division, NASA Goddard Space Flight Center, Greenbelt, MD 20771, USA
(6) Goddard Planetary Heliophysics Institute, University of Maryland, Baltimore County, Baltimore, MD, United States
(7) SSSRC, 100 Tennyson Avenue, Nashua, NH 03062, USA
(8) Catholic University of America, Washington DC, United States
(9) Graduate School of Science, Kyoto University, Kyoto, 6068501, Japan
(10) Space Physics Laboratory, Vikram Sarabhai Space Centre, ISRO, Thiruvananthapuram, 695022, Kerala, India
(11) Observatori de l'Ebre, (OE) CSIC – URL, 43520, Roquetes, Spain
(12) Department of Geophysics, National Observatory of Brazil, São Cristóvão, 20921-400, RJ, Brazil
(13) Research Institute for Sustainable Humanosphere, Kyoto University, Uji, 6110011, Japan

* hisashi@nagoya-u.jp; hisashi.hayakawa@stfc.ac.uk

Abstract

In late March 1940, at least five significant solar flares were reported. They likely launched interplanetary coronal mass ejections (ICMEs), and were associated with one

of the largest storm sudden commencements (SSCs) since the year 1868, resulting in space weather hazards that today would have significant societal impacts. The initial solar activity is associated with a short geomagnetic storm and a notable SSC. Afterward, the third flare was reported in the eastern solar quadrant (N12 E37-38) at 11:30–12:30 UT on 23 March, with significant magnetic crochets (up to ≈ |80| nT at Eskdalemuir) during 11:07–11:40 UT. On their basis, we estimate the required energy flux of the source flare as X35±1 in soft X-ray class. The resultant ICMEs caused enormous SSCs (up to > 425 nT recorded at Tucson) and allowed us to estimate an extremely inward magnetopause position (estimated magnetopause standoff position ≈ 3.4 R_E). The time series of the resultant geomagnetic storm is reconstructed using a Dst estimate, which peaked at 20 UT on 24 March at ≈ −389 nT. Around the storm main phase, the equatorial boundary of the auroral oval extended ≤ 46.3° at invariant latitudes. This sequence also caused a solar proton event and Forbush decrease (≈ 3%). These sequences indicate pileups of multiple ICMEs, which even achieved a record value of inward magnetopause position. Our analyses of this historical pioneer event bring more insights into possible serious space weather hazards and provide a quantitative basis for future analyses and predictions.

Key Words: Sun: coronal mass ejections (CMEs) – Sun: flares – (Sun:) solar-terrestrial relations – (Sun:) sunspots – planets and satellites: magnetic fields – Magnetic Fields

1 Introduction

Solar eruptions frequently release interplanetary coronal mass ejections (ICMEs). These ICMEs occasionally interact with the terrestrial magnetic field with sufficient mass, velocity, and southward interplanetary magnetic field (IMF) to cause geomagnetic storms and equatorward extensions of the auroral oval (Gonzalez *et al*., 1994; Yokoyama *et al*., 1998; Daglis *et al*., 1999; Pulkkinen, 2007). Analyses of such solar and geomagnetic storms are more than just of academic interest due to their potential to create space weather conditions that frequently enhance electric currents in space, which in turn can affect essential societal infrastructure such as power grid systems, satellite operations, and long-range communication systems (Pulkkinen, 2007; Baker *et al*., 2008; Schrijver, 2015; Pulkkinen *et al*., 2017; Riley *et al*., 2018; Raghav *et al.*, 2018, 2019; Oliveira *et al*., 2020a, 2021a; Hapgood *et al*., 2021).

Geomagnetic storms are frequently quantitatively measured using amplitudes of negative excursions in the Dst index. This index has been constructed as a proxy for the ring current intensity and has been calculated from the latitudinally-weighted average of the hourly *H* disturbances in four standard mid- and low-latitude stations since the International Geophysical Year (IGY) in 1957–1958 (Sugiura, 1964; Sugiura and Kamei, 1991). The largest geomagnetic storm recorded based on the Dst index is the March 1989 storm, which developed a minimum Dst of −589 nT. This event extended the auroral visibility down to a magnetic latitude (MLAT) of ≈ 29°, and also caused serious space weather hazards, such as a blackout of the Canadian Hydro-Québec power system, which resulted in a power shortage (Allen *et al*., 1989; Bolduc *et al*., 2002; Silverman, 2006; Boteler, 2019).

Similar space weather hazards were also reported during other great geomagnetic storms in October 2003 (minimum Dst = −353 nT and −383 nT, respectively), and in May 1967 (minimum Dst = −387 nT) (Gopalswamy *et al*., 2005; Pulkkinen *et al*., 2005; Thomson *et al*., 2005; Knipp *et al*., 2016; Meng *et al*., 2019). Such intense geomagnetic storms are rare and make statistical analyses attractive but challenging (Kilpua *et al*., 2015; Lefèvre *et al*., 2016). From 1957 onward, the standard Dst index went beyond the threshold of the minimum Dst ≤ −350 nT during only 11 geomagnetic storms (Löwe and Prölss, 1997; Table 1 in Meng *et al*., 2019).

Despite this, it is known that historical superstorms that occurred before the IGY exceeded the March 1989 storm in their magnitudes, such as those in September 1859, February 1872, and May 1921 (Silverman and Cliver, 2001; Tsurutani *et al*., 2003; Siscoe *et al*., 2006; Cliver and Dietrich, 2013; Hayakawa *et al*., 2018, 2019b, 2020b, 2021c, Love *et al*., 2019b; Blake *et al*., 2020). The occurrence of future geomagnetic superstorms of similar magnitudes could be catastrophic to modern society owing to an increasing dependence on technological infrastructure (Baker *et al*., 2008; Hapgood, 2017; Oughton *et al*., 2017; Riley *et al*., 2018; Hapgood *et al*., 2021). Further investigations into historical archives have extended Dst estimates (hereafter Dst*) for other extreme storms in the past and reconstructed the magnitude and time series of several geomagnetic superstorms (minimum Dst* ≤ −500 nT) that occurred in October–November

1903, September 1909, and March 1946 (Hayakawa *et al*., 2019a, 2020a, 2020b; Love *et al*., 2019a), as well as several other extreme storms (minimum Dst* ≤ −250 nT) in November 1882, January 1938, and March 1941 (Love, 2018; Hayakawa *et al*., 2021a, 2021b).

In this context, the March 1940 storm resulted in significant contemporary interest in space weather effects on the power/communication system (Davidson, 1940; Germaine, 1940; McNish, 1940; Nicholson, 1940) and has often been cited as a groundbreaking pioneer, *i.e.*, as the first of such cases, within the history of space weather events (*e.g.*, Boteler, 2001; Boteler and Pirjola, 2014; Lanzerotti, 2017). The time series of its space weather effects in the North American sector has been analysed in terms of their time series and geographic extent (Boteler, 2001; Lanzerotti, 2017).

This storm is also associated with the largest storm sudden commencement (SSC) recorded at the Service on Rapid Magnetic Variations (SRMV) in 1869–2020 (*e.g*., Curto *et al*., 2007)[1], at Kakioka during the period 1923–2013, and at Colaba-Alibag in 1868–1967, which indicates one of the most extreme jumps in the solar wind dynamic pressure (Araki, 2014). This storm was clearly intense, ranking eighth in the *aa* index from 1868 to 2010 (Lefèvre *et al*., 2016), second in the Kakioka Event Database from 1924 onward[2], and the fifth in the Greenwich-Abinger magnetograms in 1874–1954 (Jones, 1955).

However, despite its significance, the lack of Dst index data for the 1940s makes a quantitative analysis a challenge (Balan *et al*., 2019). Such extreme geomagnetic storms (including this storm) have frequently been recorded incompletely, as their extraordinary magnitudes exceed the recording range of early magnetograms (Love *et al*., 2019a). In fact, unlike other magnetograms, the hourly *H* values at San Juan (SJG), one of the standard Dst stations, are uncertain for 3 h (16–18 UT) and for 5 h (19–23 UT) around the storm peak recorded in other magnetograms on 24 March 1940, as distributed by the World Data Center (WDC) for Geomagnetism at Kyoto. This uncertainty probably comes from off-scale or loss of its measurement, as inferred from the 4-h data

[1] http://www.obsebre.es/en/rapid
[2] https://www.kakioka-jma.go.jp/obsdata/Geomagnetic_Events/Events_index.php

gap during 15–18 UT at Tucson (see Table 1), with the "trace going off the sheet at the bottom" (Hershberger, 1940, p. 228). This problem has challenged any estimates using the existing Dst stations (Karinen and Mursula, 2005; Mursula *et al*., 2008) owing to contemporary off-scale measurements (Riley, 2017), as was the case with other historical extreme storms before the IGY (Love *et al*., 2019a, 2019b; Hayakawa *et al*., 2020a, 2020b, 2020c). Therefore, in this article, we reconstruct the chronological sequence of this space weather event from its solar origin to terrestrial impacts. Based on historical archives of solar, magnetic, auroral, and cosmic-ray observations, we have estimated the terrestrial impacts of the solar flares and ICMEs in March 1940, represented by the subsequent SFEs, SSCs, inward magnetopause motion, geomagnetic storm intensity, equatorial extent of the auroral oval, and cosmic-ray variations.

2 Solar Eruptions

2.1 Observations

The 1940 solar-terrestrial storm occurred in the declining phase of solar cycle 17 after reaching its maximum in April 1937 (table 1 of Hathaway (2015); figs. 2 and 11 of Clette and Lefèvre (2016)). According to D'Azambuja (1940), the Sun was notably eruptive in March 1940. In this context, the sunspot group 26 – namely the sunspot group AR RGO 13555 (see Fig. 1) – was notably associated with at least four clusters of approximately class 3 flares (Hα flaring area: > 600 MSH (millionths of the solar hemisphere)) and eight clusters of approximately class 2 flares (Hα flaring area of 250–600 MSH) within the contemporary Hα flare patrols (D'Azambuja, 1940; Švestka, 1976). According to the dataset for the solar sunspot regions in the National Centers for Environmental Information (NCEI)[3], this sunspot group first appeared in the eastern solar limb on 19 March and was last witnessed in the western solar limb on 1 April. It crossed the central meridian on 26 March (Newton, 1940), and its area developed up to 1599 MSH on 30 March.

[3] https://www.ngdc.noaa.gov/stp/solar/sunspotregionsdata.html

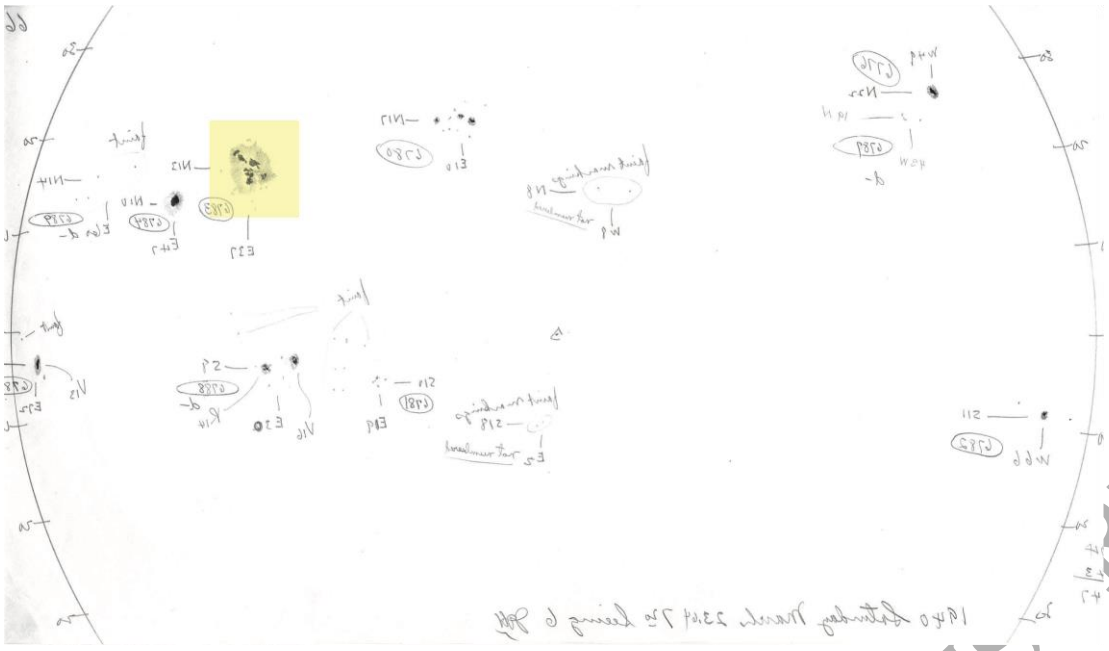

Figure 1: The solar disk on 23 March 1940, captured at Mt. Wilson Observatory, with a corrected side-inversion (Pevtsov *et al*., 2019a). The sunspot AR RGO 13555 (= AR MWO 6783) is emphasised with a yellow square. Here, the image is side-corrected, to show the solar disk as seen in the sky. Image courtesy of Mt. Wilson Observatory.

The probable source flare of the extreme geomagnetic storm on 24 March 1940 was considered a solar flare at N12 E37-38 from the centre of the solar disk on the previous day, 23 March (Newton, 1940), when the sunspot area reached 1017 MSH. This flare was recorded at a minimum of three observatories, *i.e*., in Greenwich (class 3), Zürich (class 3), and Cambridge (class 2+), according to D'Azambuja (1940). Newton stated the Greenwich observation as follows: "On March 23, when the spot was 37° east of the central meridian a brilliant chromospheric eruption was seen at Greenwich (observer, Laurie) to be in progress 11^{h} 30^{m} U.T. Clouds stopped the observations at 11^{h} 45^{m}," (Newton, 1940, p. 131). At Zürich, Brunner observed this flare from 11:30 UT to 12:20 UT, describing the end of this eruption as 13:30 UT. At Cambridge, Archenhold continued observations from 11:44 UT to 12:30 UT "when the eruption had decreased considerably in brightness" (Newton, 1940, p. 132). Newton (1940, p. 132) located its peak at 11:30 UT and described the Hα flaring area as approximately 750 MSD (millionths of the solar disk) in the projected area and approximately 500 MSH in the corrected area, which seems slightly smaller than described classification of class 3 (250 – 600 MSH) in D'Azambuja (1940).

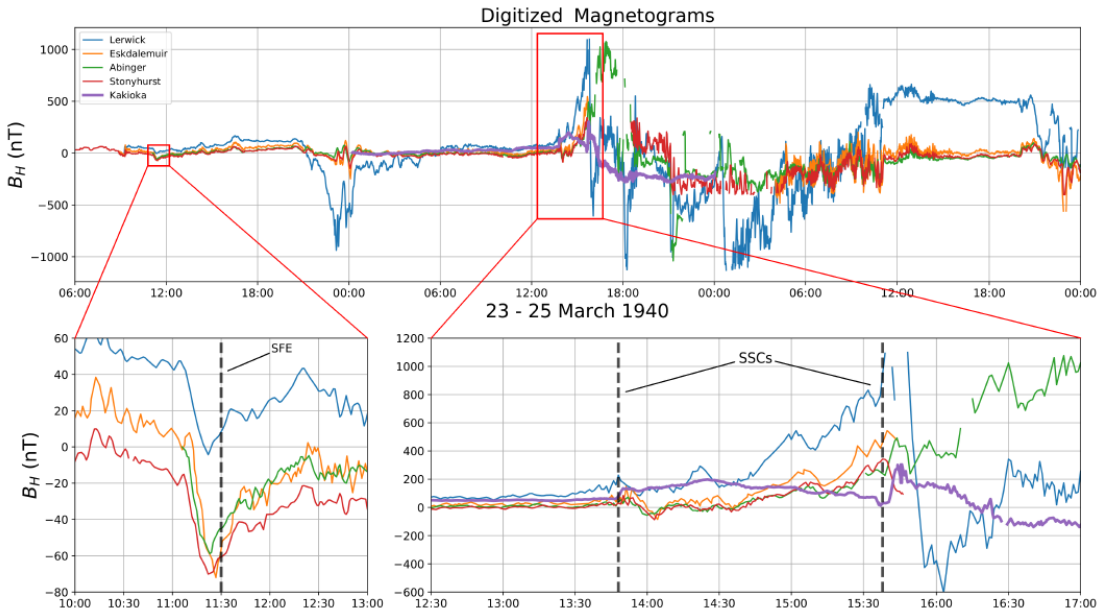

Figure 2: Horizontal magnetic field values measured at British magnetic observatories on 23 – 25 March 1940 and Kakioka magnetogram for 24 March 1940. The SFE on 23 March and the SSCs on 24 March are shown in closer detail on the bottom subplots, with dashed vertical lines indicating the reported SSC onsets as shown in the SRMV database.

It is known that intense flares often leave quasi-simultaneous footprints in the terrestrial ionosphere, as reviewed in Curto (2020). This was also the case with the major solar flare on 23 March 1940. At the time of this flare, "a complete fade-out on long distance short-wave wireless transmission on channels within the Earth's sunlit hemisphere" occurred, which started at 11:08 UT and affected all stations of Cable and Wireless Ltd. by 11:14 UT and lasted for ≈ 1.25 h (Newton, 1940, p. 132; see also Ellison, 1940). This is also confirmed by the magnetic crochets, *i.e.*, solar flare effects (SFEs), in the British magnetograms at that time (McIntosh, 1951; Jones, 1955), resulting from radiation enhancements mainly in X-rays and EUV emissions during this solar flare. Fig. 2 shows the time series of these magnetic crochets and the resulting SSCs, computed from British magnetograms digitised in the British Geological Survey (BGS). Here, the British magnetograms at Abinger, Eskdalemuir, Stonyhurst, and Lerwick show large magnetic crochets with amplitudes of |59| nT, |80| nT, |55| nT, and |52| nT, respectively (*c.f.*, Jones, 1955; McIntosh, 1951). Their durations span from 11:07 to 11:40 UT, their max-

imum excursions are located at 11:24 UT and occurred before the beginning of the optical flare observations. Therefore, contemporary flare patrols likely missed their greatest development.

2.2 Estimation of the Soft X-Ray Fluxes of the Source Flare

No direct measurements for the soft X-ray energy (SXR) fluxes are known for this flare, as satellite observations did not exist at that time. However, it is also known that the SXR fluxes in the GOES classification[4] of the solar flares empirically correlate with the resultant SFE amplitude, whereas it also depends on the solar zenith angle at the observational site (Curto *et al*., 2016; Curto, 2020). Curto *et al*. (2016) have established an empirical model of their relationship. As described in Curto *et al*. (2016), this model estimates the X-ray radiation from the perturbations they produce at the Earth by the SFEs. First, an empirical relationship between the variation in the radiation (cause) and its effect on the magnetism (consequence) was established. Then, using the inverse function (equation 4 in Curto et al., 2016), we have estimated the energy flux of the source flare. In this equation, α and β parameters were found through an iterative process as explained in Curto *et al*. (2016). It is worth noting that in cases like this, when EUV was not available, an empirical relationship between X-ray and EUV given in Le *et al*. (2011) was used, so that this estimate of the EUV term was integrated in this equation.

Among the British magnetograms shown in Fig. 2, the greatest SFE (|80| nT) was recorded at Eskdalemuir. According to Curto *et al*. (2016), the source flare needs SXR fluxes of X35±1 to produce such large SFEs. We have modelled the time series of the flare SXR flux, following the minute-data in the Eskdalemuir ΔH (Fig. 3). Caveats must be noted here, as the timings of its onset (11:07 UT) and end (11:40 UT) are slightly subjective because a waving signal of ≈ 10 nT is present before the flare onset and overlaps the SFE decrease. Still, this energy flux exceeds those of the greatest solar flares in the modern observations from 1976 onward, namely those of 16 August 1989 (X20) and 2 April 2001 (X20), possibly compares with that of 4 November 2003 (> X28 and probably X35 to X46) (Cliver and Dietrich, 2013; Curto *et al*., 2016; table 2.3 of Miyake *et*

[4] Its operation has been conducted with the observations of GOES (Geostationary Operational Environmental Satellite).

al., 2019). The SXR fluxes for the March 1940 flare were most probably not as much as those of the Carrington flare on 1 September 1859 (X45±5 in Cliver and Dietrich (2013)), which were estimated as X46±2 in Curto *et al*. (2016) following the same procedure.

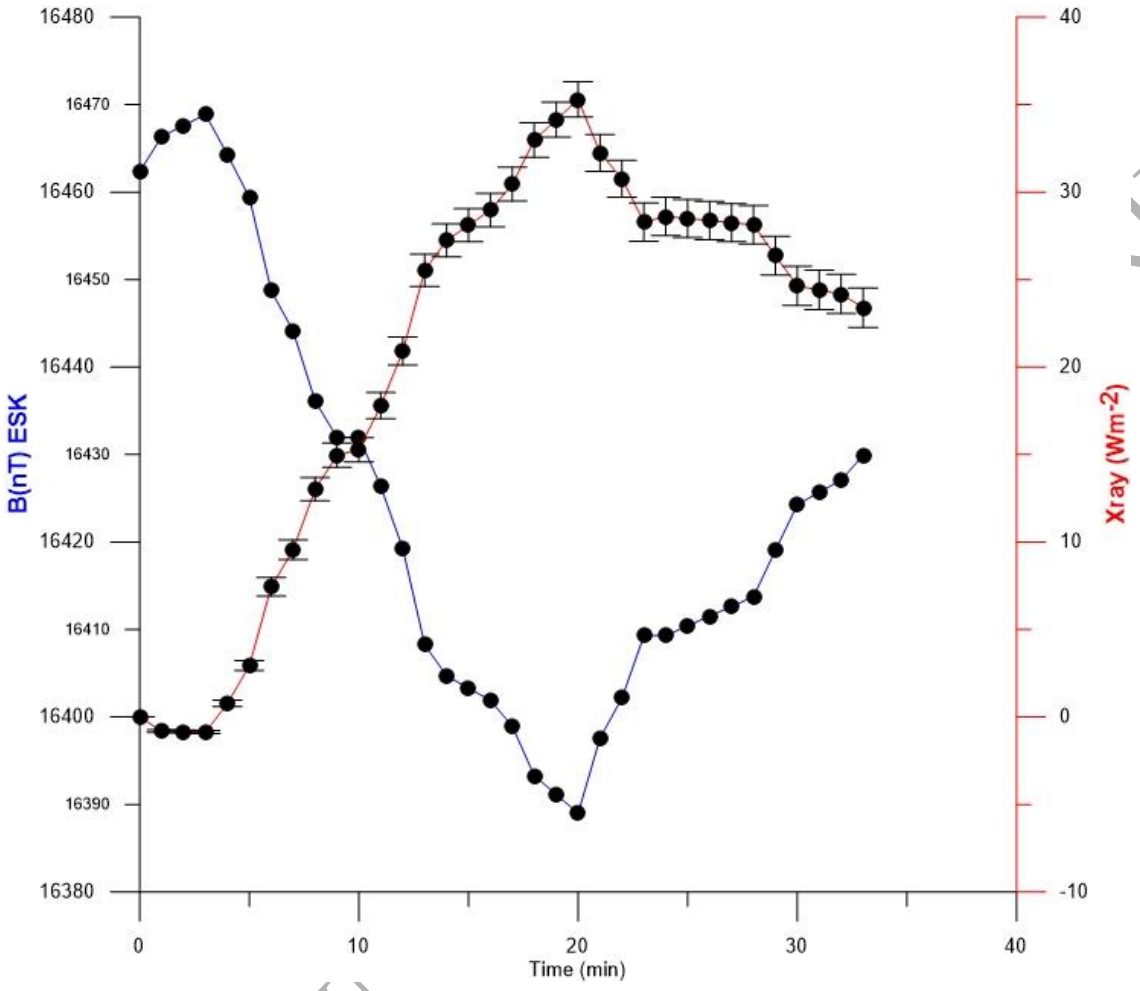

Figure 3: Time series of the extreme SFE reported at Eskdalemuir Δ*H* (blue curve) and the modelled SXR flux of the source solar flare (red curve), following Curto *et al*. (2016). This time series starts from 11:07 UT and ends at 11:40 UT.

3 Interplanetary Coronal Mass Ejections

3.1 Observed SSCs

After these solar eruptions, the interplanetary space was disturbed by multiple ICMEs. At least two SSCs were recorded on 24 March. These SSCs occurred at 13:48 UT and 15:38 UT, according to the SRMV Database. We have surveyed their contemporary

records from four mid-latitude stations. We have summarised the reported SSC amplitudes and storm amplitudes (spot values) along with their observational sites and source documents in Table 1. The geographic and geomagnetic positions of these stations are shown in Fig. 4 for 15:38 UT. This summary has expanded the SSC data from the results of Araki (2014), revising the existing data and increasing new data with contemporary reports. Contemporary data show that the SSC amplitudes are slightly larger at Alibag and Cape Town than those in Araki (2014). We have also digitised the Kakioka magnetogram on 24 March 1940 in Fig. 2 and derived the corresponding SSC amplitudes: (72 nT for SSC1 and > 276 nT for SSC2) with what Araki (2014) has shown (73 nT for SSC1 and > 273 nT for SSC2). Here, we need to emphasise that these reports frequently remain verbal and tabulated without graphical measurements. Only few of their original magnetograms have been publicly accessible and some have been probably lost (*e.g.*, Araki, 2014, p. 2), confirming the urgent need of preservation and digitisation of such historical records (Pevtsov *et al*., 2019b). As summarised in Table 1, we have located five mid-latitude reports for SSC1 (13:48 UT) ranging from 34 nT to 74 nT and four mid-latitude reports for SSC2 (15:38 UT) ranging from 198 nT to > 425 nT.

Table 1: Amplitudes of the two large SSCs at 13:48 UT and 15:38 UT and the geomagnetic storms on 24 March 1940 recorded by the individual low/mid-latitude magnetograms (< |45|° MLAT). The abbreviations used are as follows: LAT (geographic latitude), LON (geographic longitude), MLAT (magnetic latitude), MLON (magnetic longitude), SSC1 (the SSC at 13:48), and SSC2 (the SSC at 15:38). The local storm amplitudes at individual stations are shown not in hourly averages but in absolute spot values.

Observatory	LAT	LON	MLAT	MLON	SSC1 (nT)	SSC2 (nT)	Storm (nT)	References
Kakioka	N36°14′	E140°11′	26.0	−154.5	72	> 276	661	KED; Fig. 2
Alibag	N18°39′	E072°52′	9.5	143.2	62	321	> 785	Rangaswami 1940
Cape Town	S33°57′	E018°28′	-32.6	79.4	34	198	606	Ogg 1941
Tucson	N32°10′	W110°44′	40.3	−48.3	74	> 425	> 869	Hershberger 1940
Watheroo	N30°19′	E115°52′	18.8	−176.0	55		685	Parkison 1940
Huancayo	S12°02′	W076°20′	-0.6	−7.7			1395	Wells 1940

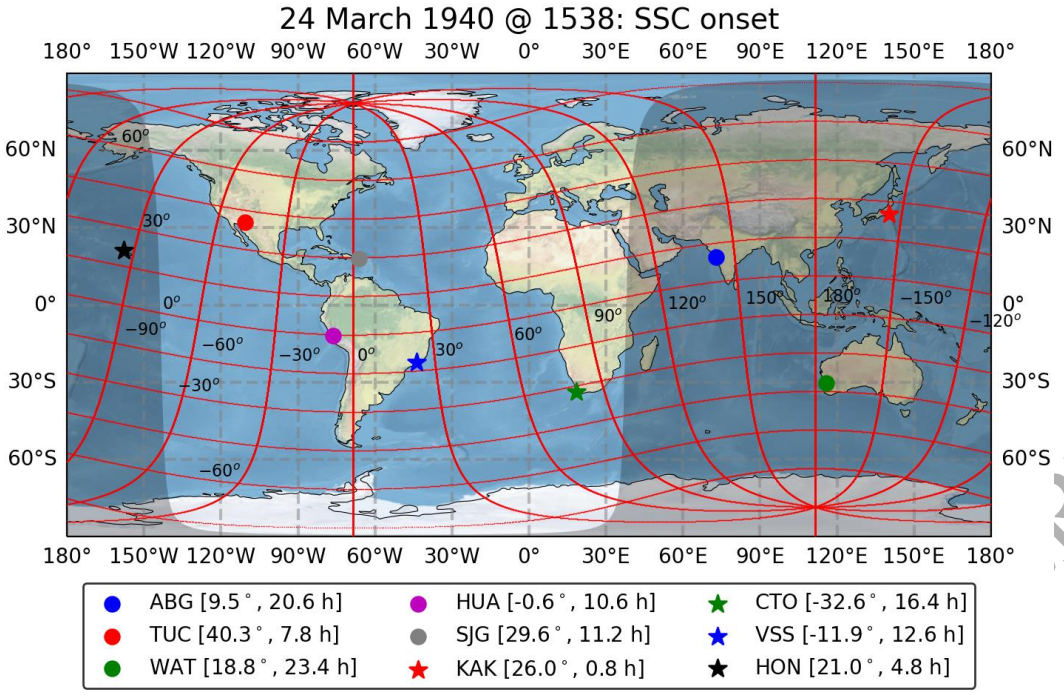

Figure 4: Geographical distributions of the magnetograms in Table 1, which recorded the SSCs at 15:38 UT on 24 March 1940 (SSC2). The thick red lines indicate centred dipole magnetic latitudes and longitudes, whereas the shaded areas indicate nightside local times. The parameters shown between squared brackets are the magnetic latitude and magnetic local times for the respective station at 15:38 UT. Here, we follow the WDC abbreviations for each station: ABG (Alibag), HUA (Huancayo), CTO (Cape Town), TUC (Tucson), SJG (San Juan), VSS (Vassouras), WAT (Watheroo), KAK (Kakioka), and HON (Honolulu).

3.2 ICME Transit Times

We associate the first SSC with a cluster of flare reports at N10-12 E40-42 during 01:33 – 02:28 UT on 23 March (D'Azambuja, 1940, p. 47) and compute their average speed as 1160 km/s (ICME1). It is reasonable to association the second SSC with the reported class-3 solar flare at 11:30–12:20 (*e.g.*, Newton, 1940; Araki, 2014) and its synchronised SFEs at 11:07/08–11:40 (Fig. 2). Based on the SFE maximum at 11:24 (SFEs), the ICME transit time is calculated as 28.2 h. This allows us to estimate their average speeds as 1470 km/s (ICME2). Its fast transit is comparable to other fast ICMEs in the observational history (*e.g.*, Cliver *et al.*, 1990; Gopalswamy *et al.*, 2005; Freed and Russell, 2014). Additionally, assuming drag effects caused by the ambient solar wind

density reduce ICME speeds uniformly by 35% from near the Sun to around 1 au (Kay *et al.*, 2020), both average velocities would be 17.5% greater near the Sun, *i.e.*, 1360 and 1730 km/s, respectively. Equivalent ICME speeds were observed a few times by Ravishankar and Michałek (2019) even during the ascending phase of the relatively weak Solar Cycle 24. Therefore, such ICME speeds are not extremely rare.

3.3 Further SSCs in late March

Even after these storms, AR RGO 13555 continued to produce major flares including two class 3 flares on 27 and 30 March and caused another set of twin geomagnetic storms. A class 3 flare at N12 W40 on 27 March (17:10 – 17:45 UT) was reported at Sherborne (D'Azambuja, 1940, p. 48; Ellison, 1940). This flare is probably associated with the SSC at 16:03 UT on 29 March initiating a series of geomagnetic disturbances lasting three days (see SRMV Database and Kakioka Event Database). The flare was the brightest eruption of its kind observed with the Sherborne spectrohelioscope at that time; associated effects at the earth included a wireless fade-out lasting from 16:19 until 18:30 UT indicative of another powerful solar eruption (Ellison, 1940). For this ICME (ICME3), the average transit time to Earth was 46.5 hrs and yielded an average speed of 890 km/s.

Another powerful flare (class 3) was recorded at N15 W54 on 30 March at Watheroo (01:00 – 02:00 UT) and Kunming (01:15 – 02:07 UT) (D'Azambuja, 1940, p. 48). This flare has now been attributed as the source of the SSC at 09:41 UT on 31 March in the SRMV Database and Kakioka Event Database (see also Jones, 1955, p. 81). For this ICME (ICME4), its average transit time to Earth was 32 hrs and yielded average velocity of 1300 km/s. These last ICMEs (ICME3 and ICME4) resulted in another sequence of intense geomagnetic storms. While this article concentrates on the period 21 – 25 March 1940, we note that AR RGO 13555 continued to dominate the near-Earth space environment for several days after the extreme event on 24 March.

4 Estimates of Subsequent Geospace Response

4.1 SSC Amplitudes

The recorded amplitudes of the SSC2 at 15:38 were exceptionally enormous, as summarised in Table 1 and Section 3.1. These SSC amplitudes were the smallest at Cape Town

and the largest at Tucson. Local times here probably played a major role in defining the Dst* estimates. Therefore, we should discuss this in light of the stations' magnetic local times (MLTs), indicated in Fig. 4, whose shaded areas indicate night times. Upon the second SSC occurrence at 15:38 UT, Tucson and Cape Town were located approximately around the post-dawn and mid-afternoon regions, with MLTs ≈ 8 h and ≈ 16 h, respectively. Within a time interval of less than 2 h, both shocks most likely hit the magnetosphere in the morning sector with large shock impact angles and high speeds (Oliveira and Samsonov, 2018; Oliveira *et al*., 2018), which explains why the SSC amplitude at Tucson was much larger than that at Cape Town, since Tucson may have been approximately in the path of the highly inclined shock (Rudd *et al*., 2019; Oliveira *et al*., 2020b). In addition, these shocks may have hit the Earth's magnetosphere with high inclination in the meridional plane as well (Xu *et al*., 2020). The large-amplitude disturbances on the nightside (Kakioka and Alibag) can be explained by the significant contribution from ionospheric currents and field-aligned currents (*e.g.*, Araki *et al*., 2006, Vichare *et al.*, 2014). On this basis, we have calculated the spot Dst* estimate for the initial SSC (13:48 UT) and the second SSC (15:38 UT) as ≈ 70 and ≈ 356 nT, respectively. Because the second SSC amplitudes at Kakioka and Tucson were incompletely recorded, our Dst* estimate for the second SSC should be regarded as a conservative estimate.

4.2 Estimates for the Terrestrial Impacts

As summarised in Equation (1), the solar wind dynamic pressure has a fairly good empirical correlation with the spot Dst value of the associated SSC (Siscoe *et al*., 1968; Burton *et al.*, 1975):

$$\Delta P_d[\mathrm{nPa}] = 4.0 \times 10^{-3} Dst^2 \quad \ldots \qquad (1)$$

Following this equation, we calculate the jumps of the solar wind dynamic pressures for the initial shock and the second shock as $\Delta P_{d1} \approx 19.7$ and $\Delta P_{d2} \approx 507.5$ nPa, respectively. Considering nominal solar wind conditions (speed 450 km/s, number density 5 cm^{-3}), the nominal solar wind ram pressure is $Pd_0 = 1.69$ nPa. Thus, $Pd_1 = \Delta Pd_1 + Pd_0 = 21.3$ nPa. The magnetosphere can be highly compressed by an inclined shock for ≈ 2 h as

shown by Oliveira *et al*. (2021b) for a strong shock occurring on 20 September 2015. Then, assuming the magnetosphere was highly compressed by ICME1 when ICME2 impacted Earth, $P_{d2} = \Delta Pd_2 + Pd_1 = 528.9$ nPa. These values are quite extreme in comparison with the usual ram pressure of a quiet solar wind (≈ 1.69 nPa) for the same solar-wind condition. In fact, those for ICME1 and ICME2 were approximately 15- and 394-times larger, respectively. Caveats must be noted here, as the IMF polarity also influences these estimates. This profile is missing, as satellite measurements did not exist at that time.

We have also assumed equilibrium conditions of the solar wind interaction with the terrestrial magnetic pressure and derived the inward magnetopause position using the empirical equation (see Baumjohann and Treumann, 2009):

$$X_{mp} = \left(\frac{KB_0^2}{2\mu_0 P_d} \right)^{1/6} \quad \ldots \quad (2)$$

Here, B_0 describes the dipole terrestrial magnetic field at $L = 1$, which is considered as 32286 nT following the IGRF-12 model for the year 1940 (Thébault *et al*., 2015). In addition, K and μ_0 represent an arbitrary factor and the vacuum magnetic permeability ($4\pi \times 10^{-7}$ H/m), respectively. We assume that $K = 2$ (Baumjohann and Treumann, 2009) and apply P_{d1} and P_{d2} in equation (1) to obtain the magnetopause positions at the subsolar point (X_{mp}). These values are calculated as 5.8 R_E and 3.4 R_E for the first and second shocks, respectively. The time interval between the first and second shocks was ≈ 110 min. These estimated magnetopause standoff positions surpassed the geosynchronous orbit (≈ 6.6 R_E) and the orbit of Global Positioning System satellites (≈ 4.2 R_E), which would expose modern satellites to the harmful solar wind environment and possibly damage their vital electronic systems beyond repair (*e.g.*, Koons and Fennel, 2006; Baker *et al*., 2017).

The extremely large amplitudes of SSC2 (Table 1) indicate that the solar wind dynamic pressure was probably quite high due to the arrival of the shock driven by ICME2. Likewise, the magnetopause position should be $X_{mp} = 3.87$ R_E very close to our estimate, even if we use Araki's (2014) estimate for the P_d increase of ≈ 457 nPa using a

conservative SSC amplitude of ≈ 277.95 nT. Caveats must be noted here, as these estimates can be affected by the IMF B_z polarity and strength, upon which the magnetopause positions are dependent (Shue *et al*., 1998), as we discuss below.

Our computation result for the ICME2 far surpasses the reported most inward magnetopause motion to ≈ 5.24 R_E (Hoffmann *et al.*, 1975) during the fastest ever observed ICME of August 1972 (Vaisberg and Zastenker, 1976; Cliver *et al*., 1990; Knipp *et al*., 2018). Additionally, Tsurutani and Lakhina (2014) used theoretical and empirical assumptions to estimate the most extreme ICME within the Sun's capability. Accordingly, its consequent impact on Earth was used to estimate the resulting most inward standoff magnetopause position as $X_{mp} \approx 5\ R_E$. The same parameters were applied in global magnetohydrodynamic simulations by Welling *et al*. (2021), who found $X_{mp} \approx 2.84\ R_E$. Numerical simulations conducted by Blake *et al*. (2021) used solar wind and IMF conditions of an extreme event (20 November 2003) scaled to Carrington-like magnitudes to find that the magnetopause standoff position was forcedly pushed inward to $X_{mp} \approx 2.26\ R_E$. Therefore, while our calculated magnetopause standoff position for this event is closer than has ever been measured, it does not exceed previous simulations and experimental data results for extreme geomagnetic storms.

Another interesting point to consider is that the magnetosphere was highly perturbed during the arrival of ICME2. According to Vaisberg and Zastenker (1976), the August 1972 CME had an average speed of 2850 km/s, pushing the magnetospause standoff position to ≈ 5.24 R_E, under dynamic pressure of ≈ 25 nPa (see also Gopalswamy *et al*., 2005; Freed and Russell, 2014). However, the second ICME on 23 March had a relatively modest average speed of 1470 km/s with dynamic pressure of ≈ 528 nPa, which led the magnetopause standoff position to the final position of ≈ 3.4 R_E. Additionally, had it stood alone, the impact of ICME2 would probably have been less severe, even though ICME1 most likely paved the way for ICME2 by reducing the ambient solar wind density as it usually occurs during successive ICME impacts (Gopalswamy *et al*., 2005; Liu *et al*, 2014; Wu *et al.*, 2019). This conclusion contrasts with the conclusions of Lakhina and Tsurutani (2016) regarding the March 1989 superstorm: a storm main phase continued to develop while multiple ICMEs most likely impacted the magnetosphere (See their Fig. 2).

5 Geomagnetic Storms

After the occurrence of these extremely large SSCs at 13:48 UT and 15:38 UT, the terrestrial magnetic field was significantly disturbed and an extremely intense geomagnetic storm was recorded in contemporary magnetograms, even in mid- to low-magnetic latitudes (MLATs), as summarised in Table 1. The disturbance was particularly fast and intense in the American sector, likely because it was located on the dusk side during this storm, and the local geomagnetic disturbance was enhanced. At Huancayo (HUA), this disturbance was recorded as 1395 nT and was the largest disturbance since its operation onset in 1922 (Wells, 1940). At Tucson, "for about three hours the D- and H-traces are so confused that it is impossible to tell exactly what happened, but it appears that H increased at least 425 gammas within a very few minutes, and immediately decreased equally rapidly, the trace going off the sheet at the bottom" and the "total downward plunge was at least 869 gammas, and probably a good deal more than that" (Hershberger, 1940, p. 228). This resulted in a 4-h data gap during 15–18 UT. Likewise, as stated above, the San Juan (SJG, N18°07', W066°09′; 29.6° MLAT, 2.6° MLON)) *H*-trace shows problematic data remaining at 27050 nT during 16–18 UT and at 27030 nT during 19–23 UT[5] and probably missed the peak of this geomagnetic storm.

The Dst index is computed using the hourly average of the geomagnetic disturbances of four mid-latitude stations: Kakioka (KAK) in Japan; Hermanus (HER) in South Africa; San Juan (SJG) in Puerto Rico; and Honolulu (HON; N21°19', W158°00′; 20.0° MLAT, -94.0° MLON) in Hawaii. Even if we attempt to compute the Dst time series, the SJG data problem directly affects any existing attempts to extend the Dst index or its equivalence with the standard Dst stations (Riley, 2017; Karinen and Mursula, 2005; Mursula *et al*., 2008). Therefore, we searched for low- to mid-latitude magnetograms without significant data gaps at that time to substitute this incomplete record. This is because the use of the replacement magnetogram allows us to approximate Dst estimates, as shown in several modern geomagnetic storms (fig. 2 in Love *et al*. (2019b); fig. 3 in Hayakawa *et al*. (2021a)). Here, we exclude HUA from our survey because it was too close to the geomagnetic equator (−0.6° MLAT) and hence to the equatorial electrojet. In this re-

[5] http://wdc.kugi.kyoto-u.ac.jp/index.html

gard, the Vassouras (VSS) magnetogram in Brazil recorded this geomagnetic disturbance without significant data gaps and was sufficiently distant from the direct influence of the equatorial electrojet (S22°24', W043°39′; −11.9° MLAT, 23.4° MLON). Therefore, for this magnetic storm, we substitute the SJG data with the VSS data to compute the Dst estimate.

Following the calculation procedure of the standard Dst index (Sugiura, 1964; Sugiura and Kamei, 1991; WDC for Geomagnetism at Kyoto *et al*., 2015), we derive the hourly disturbance (D_i (t)) at the individual reference stations (KAK, CTO, HON, and VSS; coloured stars in Fig. 4) and subtract the baseline (B_i) and solar quiet (Sq) field variations (Sq_i (t)). We compute the Dst estimate (*Dst* (t)) from their average with latitudinal weighting. Here, we have followed the slightly improved procedure to yield a better representative average (*e.g.*, Love *et al*., 2019a; Hayakawa *et al*., 2020a), whereas the standard Dst index was defined with the sum of the disturbance *H* variations divided by the sum of the cosines (Section 2.2.3. of Sugiura (1962)). Our procedures are summarised in the following equations:

$$D_i(t) = H_i(t) - B_i - Sq_i(t) \quad \ldots \quad (3)$$

$$Dst(t) = \frac{1}{4}\sum_{i=1}^{4}\frac{D_i(t)}{\cos(\lambda_i)} \quad \ldots \quad (4)$$

Here, we derive the individual hourly data for KAK, CTO, and HON from the WDC for geomagnetism in Kyoto. We have derived the hourly data for VSS from its yearbook (Da Gama, 1944) and converted the recorded local time to UT. We approximate the baseline (B_i) with the annual H means of the individual observatory by consulting the WDC for geomagnetism at Edinburgh[6]. Here, we do not use the VSS annual mean but use an average (23800 nT) of the closest quiet day before this storm on 18 March because it contradicts the data in the VSS yearbook (Da Gama, 1944). We approximate the Sq field variations (Sq_i (t)) with the diurnal variations in the five quietest days in March 1940 prior to this storm (6, 11, 15, 17, and 18 March 1940), selected using the revised

[6] http://www.geomag.bgs.ac.uk/data_service/data/annual_means.shtml

daily *aa* index (Lockwood *et al*., 2018a, 2018b). For their latitudinal weighting, we use MLATs as angular distances between the individual observatory and the magnetic pole in 1940, following the IGRF-12 model (Thébault *et al*., 2015).

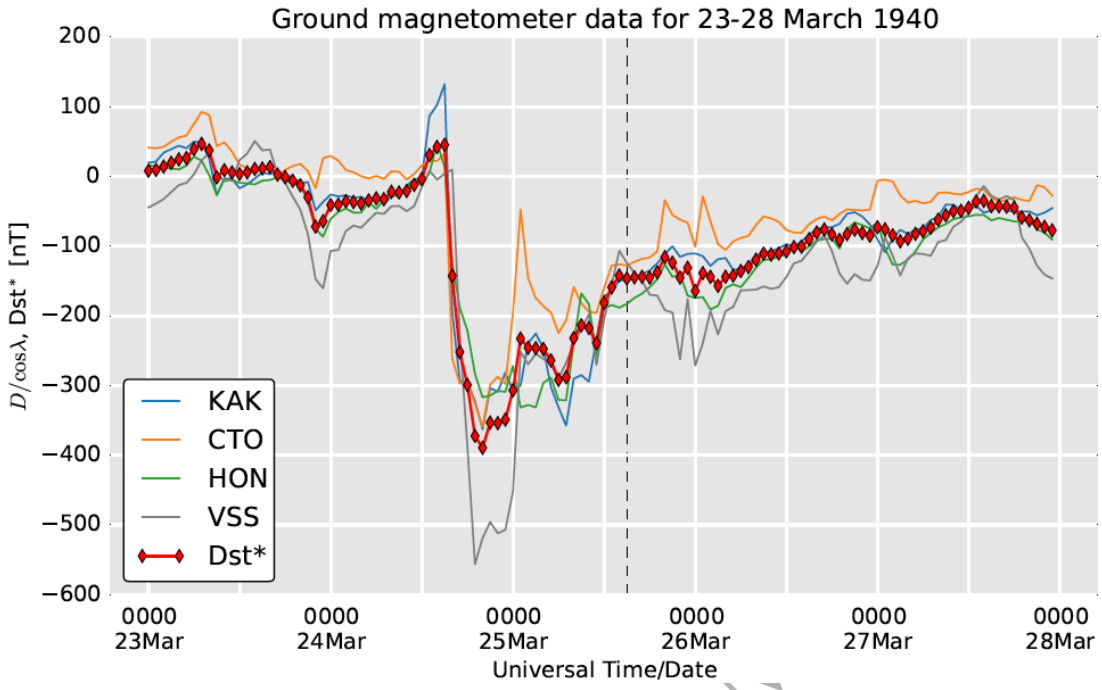

Figure 5: Dst estimate (Dst*) and the latitudinally weighted hourly disturbance (D_i (t)/cos λ_i) at the individual magnetograms (KAK, CTO, HON, and VSS), where λ_i is the respective station's magnetic latitude in March 1940.

Fig. 5 summarises the hourly disturbance (D_i(t)) with latitudinal weighting at the individual magnetograms (KAK, CTO, HON, and VSS) and their average, namely our Dst estimates (Dst*; red curve with diamonds) values. The minimum value of our Dst* is ≈ −389 nT, which was reached at 20 UT on 24 March 1940. The geomagnetic storm developed steeply for 5 h after the second SSC. The negative disturbance around the storm peak was significantly enhanced at VSS, probably because of the significant contribution from the storm-time ring current that develops mostly in the midnight-dusk sector (Cummings, 1966; Ebihara *et al*., 2002). This is consistent with the significant enhancements and scale-offs and data gaps of the local geomagnetic disturbances recorded in the North American sector, which was located on the dusk-side. The Dst* variation exhibited a two-step recovery. The rapid recovery lasted until 14 UT on 25 March (dashed black vertical line in Fig. 5). The possible cause of the two-step recovery is

thought to be different lifetimes of the charge exchange of H^+ and O^+ ions (Hamilton *et al*., 1988), precipitation of the ions that contribute to the ring current (Kozyra *et al.*, 1998), and a rapid decrease in the plasma sheet ions (Ebihara and Ejiri, 2000) and pitch angle scattering in curved field lines (Ebihara *et al*., 2011).

Its magnitude (minimum Dst* ≈ −389 nT) is categorised as an extreme storm beyond the threshold of minimum Dst ≤ −250 nT (Meng *et al*., 2019). In comparison with the extreme storms within the standard Dst index, the March 1940 storm was comparable to or slightly more intense than the March 2001 storm (minimum Dst = −387 nT) and May 1967 storm (minimum Dst = −387 nT), based on the standard Dst index, which have been ranked the sixth and seventh most extreme storms since 1957 (Gopalswamy *et al*., 2005; Huba and Sazykin, 2014; Knipp *et al*., 2016; Meng *et al*., 2019). However, the storm intensity does not exceed the second to fifth geomagnetic storms in 1957–1959 and 2003, with their intensity within the minimum Dst ranging from −429 nT to −422 nT, based on the standard Dst index[7] (*e.g*., Stanislawska *et al*., 2018; Balan *et al*., 2019; Meng *et al*., 2019; Knipp *et al*., 2021; Hayakawa *et al*., 2022). As intense geomagnetic storms tend to occur more frequently around the spring equinox (Russell-McPherron effect; Russell and McPherron, 1973; Cliver *et al*., 2004; Svalgaard, 2011; Balan *et al*., 2019), this storm (24 March) may have been benefitted from the chronological proximity with the spring equinox.

6 Low-Latitude Aurorae

Although the March 1940 storm peaked at 20 UT on 24 March, the observational conditions for the mid/low-latitude aurorae were far from ideal because of the moon phase only one day after the full moon on 23 March (Nicholson, 1940; Jones, 1955). Nevertheless, auroral visibilities were reported mainly in the European sector (Flammarion and Quenisset, 1940), probably because the storm peak met the local evening. In fact, contemporary newspapers reported auroral visibilities even as far south as Greece and

[7] Magnitudes of the top 5 geomagnetic storms are scaled in their minimum Dst as follows: −589 nT on 14 March 1989, −429 nT on 15 July 1959, −427 nT on 13 September 1957, −426 nT on 11 February 1958, and −422 nT on 20 November 2003 (WDC for Geomagnetism at Kyoto *et al*., 2015; Meng *et al*., 2019).

Turkey, Tajikistan, and Japan (*e.g.*, Plakidis, 1940; Haber, 1940-03-26, p. 4; Suiro Yoran, 1940; AN SSSR, 1954), as summarised in Fig. 6.

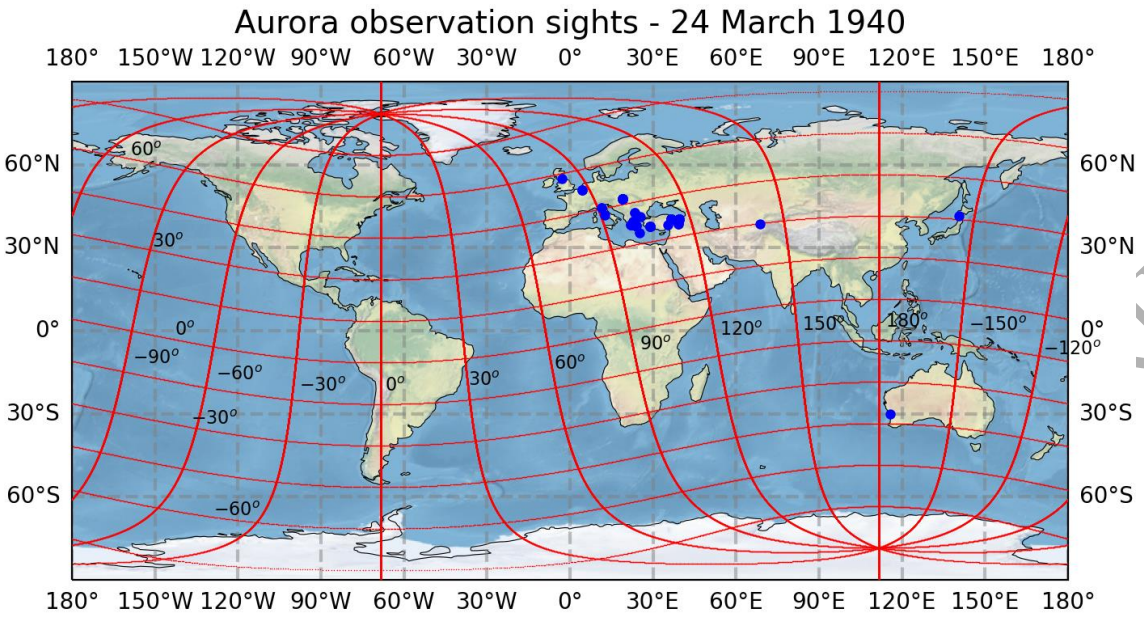

Figure 6: Auroral visibility on 24 March 1940, as extracted from the Greek and Turkish local newspapers (*e.g.*, ΤΑΧΥΔΡΟΜΟΣ ΒΟΛΟΣ, 1940-03-26, pp. 3 – 6; ΘΕΣΣΑΛΙΑ (Η)_ΒΟΛΟΣ, 1940-03-26, p. 4; Haber, 1940-03-26, p. 4) and Japanese, Tajik, and Australian reports (Suiro Yoran, 1940; Parkinson, 1940; AN SSSR, 1954).

In Greece, an auroral display was reported from Thrace to Crete. At Penteli (N38°03′, E023°52′; 36.7° MLAT), where the National Observatory of Athens is situated, the auroral display was reported during 17:30–19:30 UT. The auroral display looked like rising orange frames in combination with a thin white-yellow cloud. Its altitude was reported to be up to 20° (Plakidis, 1940, p. 418). The reported auroral visibility was chronologically located in the storm main phase to the early recovery phase (Fig. 4). The reported altitude allows us to compute the footprint of the magnetic field line of the observed equatorial auroral boundary as ≈ 46.3° ILAT (invariant latitude), assuming a visible auroral altitude of ≈ 400 km (Roach *et al.*, 1960; Ebihara *et al.*, 2017). This is a conservative estimate and can be revised with the addition of any records further equatorward. Therefore, we consider the equatorial auroral boundary as ≤ 46.3° ILAT.

Aurorae were also reported in the East Asian and Australian sector. In fact, a Japanese vessel in the Tsugaru Strait (N41°28′, E140°30′; 31.2° MLAT) reported auroral visibility at 02:57–03:05 and 03:35–03:39 in LT, namely at 17:57–18:05 and 18:35–18:39 in UT (Suiro Yoran, 1940). This report is chronologically located in the storm main phase (Fig. 5). Here, the Japanese vessel compared its visibility with light immediately before sunrise. In Australia, aurora australis was reported at Perth (S31°57′, E115°51′; −43.4° MLAT) during 17 – 20 UT, which is also contextualised in the storm main phase (Parkinson, 1940). In Central Asia, aurora borealis was reported down to Stalinabad (Dushanbe: N38°33', E068°47'; 29.7° MLAT) during this night (AN SSSR, 1954). Assuming the same equatorward extension of the auroral oval (≤ 46.3° ILAT), we expect the auroral display seen from this Japanese vessel and Stalinabad to be visible at ≥ 8° and at ≥ 6° in elevation angle, respectively.

7 Cosmic-Ray Variability

7.1 Observations with the Ionization Chambers

In the 1940s the cosmic ray intensity at Earth was primarily monitored with ionization chambers of different designs and sensitivities in various countries (Shea and Smart, 2000), while it is challenging to calibrate their data with those of the neutron monitors (McCracken, 2007; Usoskin *et al*., 2011; Shea and Smart, 2019). The Carnegie Institute operated a series of standardized ionization chambers enabling a unique comparison of the cosmic radiation over a wide rigidity range from the polar to equatorial latitudes. In 1940, these instruments were located at Godhavn (Greenland), Cheltenham (USA), Christchurch (New Zealand), Teoloyucan (Mexico), and Huancayo (Peru)[8] and were capable of monitoring the cosmic radiation above ≈ 4 GeV or the geomagnetic cutoff for mid-to-equatorial locations. At that time in history, solar proton events had not been identified. As time progressed, major ionospheric disturbances particularly in the polar ionosphere were associated with an increase in solar protons in the multi MeV range (see fig. 3 in Bailey, 1964), and it is with this understanding that we have investigated the variations in the cosmic ray intensity in late March 1940.

[8] These cosmic-ray detectors became known as the "Forbush ionization chambers" as they were operated by Scott Forbush who did extensive geomagnetic and high-energy solar particle analysis utilizing these data.

7.2 Solar Proton Event: Observations

To more fully understand these events, Table 2 (in Section 8) presents a timeline of the major solar and geomagnetic phenomena 19 – 24 March. In a list of periods of abnormal polar cap absorption/blackout events, Besprozvannaya (1962) suggested an event occurred between 22 UT (20 March) and 06 UT (21 March) as recorded by vertical incidence ionospheric sounding measurements at Tikhaya Bay (N80º19', E52º47'). Furthermore, she reported that the disturbance continued for 5 days with blackout lasting 96 hours. Švestka (1966) suggested that the solar flare at N12 E55 could have produced a solar proton event.

The *Quarterly Bulletin on Solar Activity* (QBSA) for 1940 identifies a class 2 solar flare on 21 March at 03:00 – 03:23 UT at N20 E55 recorded at Watheroo (D'Azambuja, 1940), presumably the same event identified by Švestka (1966). This flare is associated with AR RGO 13553. A SFE was identified on a Kakioka magnetogram on 21 March at 03:12-04:00 UT (Yokouchi, 1953). SFEs observed on magnetograms are attributed to ionization in the upper sunlit ionosphere generating significant current flows. This results in a distinctive signature on a magnetogram. Contemporary reports at that time indicate that this corresponds to the maximum phase of a large solar X-ray event. From these related observations we have identified the solar flare at AR RGO 13553 from 03:00 – 03:23 UT on 21 March as a source of the long-lasting solar proton event. There are good correlations between polar cap absorption and energetic solar protons in the multi MeV range (Bailey, 1964; Sellers *et al*., 1977; Smart and Shea, 1979; Shea and Smart, 1990, 2012).

7.3 Solar Proton Event: Analyses

Solar proton events from the eastern sector of the solar hemisphere are not unusual. The NOAA Space Weather Prediction Center maintains a list of solar flare active regions associated with solar proton events affecting the Earth environment. In the 39 years from 1977 through 2015 there are 230 unique solar active regions identified as initiating a solar proton event >10 MeV at Earth; 31 (13%) of these regions are between E45 and E90. The time/particle intensity profile of these events typically shows a relatively slow particle increase to a maximum intensity; the entire event can last several days. Thus a

5-day polar cap absorption event from the powerful flare at E55 on 21 March is consistent with large eastern hemisphere solar events.

While we have associated the solar activity at E55 on 21 March with a solar proton event at Earth, this solar active region was not the dominant active region on the solar disk in March 1940. AR RGO 13555 was prolific in major flare activity as it traversed the solar disk, and it was this region that is associated with the major geomagnetic disturbances recorded at Earth. Two closely timed importance 2 flares on 23 March at 01:33 and 02:09 UT and the importance 3 solar flare from this same region 10 hours later with the associated short wave fadeout and three magnetic crochets with a peak at 11:24 UT have been associated with the major geomagnetic storm on 24 and 25 March as discussed in Section 3.

At the time of the flares on 23 March, the polar ionosphere was still experiencing blackout conditions most likely resulting from the presumed particle event two days earlier (Besprozvannaya, 1962). The identification of three SFEs peaking at 11:24 UT on 23 March (Fig. 2), plus a report from Greece of short wave fadeouts in communication during the calls of Larissa station from Athens, and Sedes from Faliro around 11:45 UT on 23 March (e.g. Plakidis, 1940, pp. 418-420) implies a major X-ray event in association with the limited optical observations of solar flare activity (D'Azambuja, 1940). It is reasonable to assume that this was also a solar proton event, thus adding to the event already in progress.

7.4 Forbush Decrease: Observations

The analog records for the Forbush ionization chambers for this period have been scanned and are available at the National Centers for Environmental Information, Data Services Division, Asheville, North Carolina, USA. The ionization chambers at Godhavn, Cheltenham and Christchurch would be capable of detecting a major relativistic solar proton event with proton rigidities of ≥ 4.85 GV (equivalent to a proton energy of 4 GeV). While there is ample evidence for the existence of the multi-MeV range solar protons as indicated by the polar cap absorption, inspection of these analog records for 23 March did not indicate any evidence for high energy particle increases.

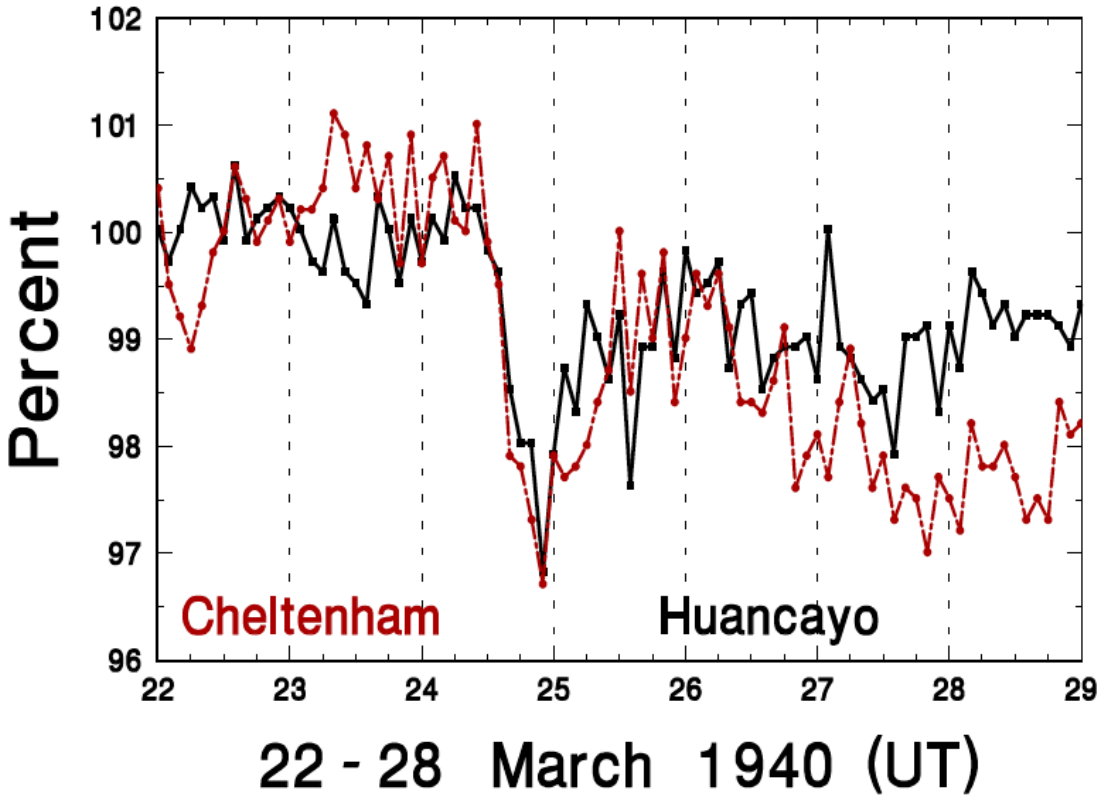

Figure 7: Bi-hourly values of the cosmic ray intensity for 22-28 March 1940 for Cheltenham and Huancayo, derived from Lange and Forbush (1948, 1957).

Bi-hourly values of the cosmic ray intensity for March 1940 for Huancayo and Cheltenham are published in Lange and Forbush (1948, 1957) respectively. These tables give the bi-hourly mean values of departures from the balance in units of 0.1% of the total cosmic ray ionization to which a constant has been applied. The data have been corrected for bursts and the barometric pressure appropriate for each location.

Using the data for 21 March 1940 as the pre-event baseline, the relative cosmic ray intensity for both detectors was calculated for the remainder of March. Fig. 7 illustrates a rapid decrease in cosmic ray intensity of ≈ 3% following the two sharp SSCs on 24 March (Table 1). This Forbush Decrease peaked at ≈ 22 UT, slightly after the peak (20 UT) of the associated geomagnetic storm. The intensity partially recovered over the next 12 hours followed by typical cosmic ray fluctuations until additional decreases occurred associated with SSCs on 29 and 30 March. In these combined events, the

cosmic ray intensity at Cheltenham was ≈ 4.5% and at Huancayo ≈ 2.2 % below the 21 March baseline.

7.5 Forbush Decrease: Analyses

The almost identical percentage decreases recorded by the Cheltenham and Huancayo ionization chambers at the maximum of the Forbush decreases on 24 March is not typical for these two detectors at different geomagnetic cutoff rigidities. The Cheltenham detector would respond to the galactic cosmic ray intensity above the detector threshold of ≈ 4.85 GV whereas the identical Huancayo detector would respond to the intensity above the geomagnetic cutoff rigidity of ≈ 13 GV. With the relatively large differences in energy response, one would expect a larger relative decrease at Cheltenham than Huancayo as observed later in March 1940 and also in the event in January 1938 (fig. 7 of Hayakawa *et al*., 2021b).

The rigidity dependences of Forbush decreases have been discussed by numerous authors (e.g. Richardson and Cane, 2011 and references therein). Belov *et al*. (2021) extensively studied the rigidity dependence during Forbush decreases using neutron monitor data and the SOHO (EPHIN) data covering a rigidity range from 1 GV to 10 GV. Fig. 9 of their paper illustrates that both detectors had similar percentage decreases during the initial several hours of the Forbush event on 27 May 2001. Shortly prior to the maximum of the decrease (minimum intensity), the rigidity dependence starts to become evident and continues during most of the recovery phase. Belov *et al*. (2021) show that the Earth was within the sheath of the ICME during the time period when there was very little rigidity dependence.

The lack of a significant rigidity dependence shown in the initial phase of the 27 May 2001 event is similar to what is observed in the initial phase of the 24 March 1940 decrease. While this type of behavior did not fit the majority of cases they investigated, Belov *et al*. (2021) emphasized that there are events that significantly differ from the mean spectral index determined from the 421 events in their study.

8 Summary and Discussions

In this study, we analysed and reconstructed the time series and magnitudes of extreme solar-terrestrial storms in March 1940. The great sunspot group AR RGO 13555 (Fig. 1) caused a major flare on 23 March at N12 E37-38 (D'Azambuja, 1940). D'Azambuja (1940) classified its Hα flare area as class 3 (> 600 MSH) at Greenwich and Zürich and class 2+ at Cambridge (≤ 600 MSH), whereas Newton (1940) derived its Hα flare area at Greenwich as ≈ 500 MSH. We consider this value to be a conservative value and estimate the flare magnitude as ≥ 500 MSH in the Hα flare area. Synchronised with this major flare, significant SFE values were reported in British magnetograms. Their magnitudes were scaled as |59| nT at Abinger, |80| nT at Eskdalemuir, |55| nT at Stonyhurst, and |52| nT at Lerwick (Fig. 2; McIntosh, 1951). As it peaked at 11:24 UT, the contemporary flare patrols likely missed its greatest development.

According to the model of Curto *et al*. (2016), in order to achieve the recorded SFE amplitudes, we estimate the energy flux for the source solar flare on 23 March as ≈ X35 ± 1 (Fig. 3). This energy flux compares the greatest solar flares captured in the instrumental observations from 1976 onward (*e.g.*, Table 2.3 of Miyake *et al*., 2019). Filling the existing data gap, this result may benefit the future discussions for the extreme solar flares and superflares (*e.g.*, Cliver and Dietrich, 2013; Curto *et al*., 2016; Karoff *et al*., 2016; Notsu *et al*., 2019; Miyake *et al*., 2019; Curto, 2020; Cliver *et al*., 2020).

Contemporary magnetograms show two large SSCs at 13:48 UT and 15:38 UT on 24 March (Table 1), indicating the arrival of significantly fast ICMEs. Assuming an association of the second SSC at 15:38 UT with the major flare and SFEs on 23 March, ICME2's transit time and average velocity were calculated as 28.2h and 1470 km/s, respectively. This SSC was extremely large and particularly enhanced in the pre-noon sector, such as in Tucson (> 425 nT), as summarised in Table 1 and Fig. 4. We estimated the spot Dst* for this SSC as ≈ 356 nT. On this basis, the jump of the solar wind dynamic pressure and the most inward magnetopause standoff position at this SSC have been estimated as $\Delta P_{d2} \approx 508$ nPa and $X_{mp} \approx 3.4$ R_E, respectively. This extremely inward position surpassed the most inward magnetopause position ever reported of ≈ 5.24 R_E in August 1972 within the satellite era observational history (Hoffmann, 1975).

Subsequently, the terrestrial magnetosphere was significantly disturbed. This was especially the case in the American sector. HUA recorded an extreme ΔH disturbance of 1395 nT, and SJG was likely saturated for hours. Because SJG, one of the Dst stations, was also probably saturated, the Dst time series could not be computed with the standard Dst stations. Therefore, we acquired VSS data and computed the Dst* time series in combination with the other Dst stations: KAK, CTO, and HON (Fig. 5). Our estimate has its negative peak located at 20 UT on 24 March 1940 and scaled its magnitude as ≈ −389 nT, as derived from the minimum value of Dst*. Located on the dusk side, the VSS magnetogram proves significant enhancements of this geomagnetic storm and explains the off-scale and data gaps of the other mid/low-latitude stations in the American sector. In comparison with the standard Dst index, this storm magnitude is ranked between the sixth and seventh most extreme storm since 1957, based on the standard Dst index.

This extreme geomagnetic storm extended the auroral oval significantly equatorward. Despite the unfavourable conditions immediately after the full moon on 23 March, auroral visibilities were reported even as far south as Greece and Turkey. At Penteli (36.7° MLAT) in Greece, the auroral display was reported in the storm main phase (17:30–19:30 UT) at up to ≈ 20° in elevation. On this basis, we computed the footprint of the magnetic field line of the observed equatorial auroral boundary as ≤ 46.3° ILAT. This is consistent with a Japanese naval report from the Tsugaru Strait (31.2° MLAT) at ≈ 21 UT, immediately after the storm peak at 20 UT.

The contemporary cosmic-ray measurements with ionization chambers also captured notable sequence in this interval. Abnormal polar cap absorption was reported on 21 – 26 March and indicated occurrence of a significant solar proton event. As the extreme flare around 11:24 UT caused large SFEs and radio-fadeouts, this flare can be reasonably associated with an additional solar proton event, adding to the event already in progress and contributing to its long duration. The ionization chambers at Cheltenham and Huancayo show ≈ 3% decreases of cosmic-ray intensity around the occurrences of two large SSCs.

Two closely timed importance 2 flares on 23 March at 01:33 and 02:09 UT respectively are most likely the source of the SSC at 13:48 UT on 23 March; the average shock speed would be ≈ 1160 km/sec. The major solar activity from the same AR 10 hours later with an associated short wave fadeout and three magnetic crochets with a peak at 11:24 UT is most likely associated with the SSC at 15:38 UT resulting in a major enhancement of the geomagnetic storm already in progress. Typical of a second CME quickly following an initial event, the average speed of this shock at 1470 km/sec is faster than the speed of the first shock. Furthermore, AR RGO 13555 continued to produce major flares throughout the next several days presumably contributing to the polar cap absorption event that continued until 26 March. We have identified the sequence of the major solar activity periods and their associated ICME effects at Earth on 20 – 24 March including the benchmark extreme geomagnetic storm and associated Forbush Decrease in the final column in Table 2.

Table 2: Time series of major flares, SFEs, polar cap absorptions (PCAs), radio fadeouts (RFs), SSCs, Forbush decreases (FDs), geomagnetic storms (GMSs) on 20/21 – 25 March 1940. The event sequences have been noted as A, B, and C. The event A is associated with the solar proton event, which was discussed in Sections 7.2 – 7.3. The events B and C are associated with the ICME1 and ICME2, as discussed in Section 3.2.

Date	Time (UT)	Event	Magnitude	References	Notes
19	0815-0854 0910-0950	Flare	1	D'Azambuja 1940	AR13555 at N13 E90 eruptive prominence
20	1721-1736	Flare	1	D'Azambuja 1940	AR13555 at N12 E72
20/21	between 22-06	PCA (A)		Besprozvannaya 1962	For 5 days
21	0300-0323	Flare (A)	2	D'Azambuja 1940	AR13553 at N20 E55
21	0312-0400	SFE (A)		Yokouchi 1953	Max at 0313
23	0133-0147	Flare (B)	2	D'Azambuja 1940	AR13555 at N12 E42
23	0209-0228	Flare (B)	2	D'Azambuja 1940	AR13555 at N10 E40
23	0616	SSC (A)	21.0 nT	KED	Kakioka ΔH
23	~1145	RF (C)		Plakidis 1940	in Greece
23	1107-1140	SFE (C)		Fig. 2	peak at 1124
23	<1130-1230	Flare (C)	3	D'Azambuja 1940	AR13555 at N12 E37
23	<1513	Flare (C?)	>>1	D'Azambuja 1940	AR13555 at N13 E32
24	1348	SSC (B)	53.0 nT	Table 1	Dst*
24	1538	SSC (C)	263.3 nT	Table 1	Dst*
24	~20	GMS (C)	-389 nT	Fig. 5	Dst*

24	~22	FD (C)	~3%	Fig. 7	

This sequence probably indicates that the ICMEs piled up and caused a 'perfect' storm (see Liu *et al*., 2019). Similar cases are found in modern observations around the Hydro-Québec storm in March 1989 (Boteler, 2019) and the Halloween sequence in October 2003 (Mannucci *et al*., 2005), where the preceding ICMEs swept the interplanetary space reducing drag forces which in turn enhanced the following ICMEs' geoeffectiveness (Tsurutani and Lakhina, 2014; Shiota and Kataoka, 2016). The earlier ICME (ICME1) arriving at the Earth caused a large SSCs at 13:48 UT on 24 March 1940, and probably swept the interplanetary space, preconditioning the arrival of ICME2, which caused the extremely large SSCs at 15:38 UT on 24 March and subsequently an extreme geomagnetic storms of minimum Dst* ≈ −389 nT.

Interestingly, this storm sequence also caused great space weather hazards in the United States and even enhanced contemporary interest in the social impacts of geomagnetic storms (Boteler, 2001; Lanzerotti, 2017). Although its minimum Dst* was not as extreme as those of other historical superstorms, the geomagnetic disturbance was locally enhanced in the American sector (Fig. 5) and probably caused significant geomagnetically induced currents in the United States (Lanzerotti, 2017). Parallel examples can be found in Knipp *et al*. (2018). In the Mediterranean sector, short-wave disruptions were reported even as far south as Jaffa (N32°03′, E034°45′; 28.8° MLAT) and Jerusalem (N31°47′, E035°14′; 28.4° MLAT), according to local newspapers (al-Difāʿ, 1940-03-27; HaAretz, 1940-03-27). In the East Asian sector, telegraph disruptions were reported as far south as Manchuria such as Mukden (N41°48′, E123°27′; 30.5° MLAT) around 4 – 15 UT on 24 March 1940, according to the local newspapers (Manshu Nichinichi Shinbun, 1940-03-27, p. 7).

ICME2's hypothesised modern impact would be even more serious, as the estimated inward magnetopause standoff position ($X_{mp} \approx 3.8\ R_E$) surpassed the geosynchronous orbit ($\approx 6.6\ R_E$) and the orbit of the Global Positioning System ($\approx 4.2\ R_E$) and hence would expose modern satellites to the harmful solar wind environment and possibly damage their vital electronic systems (*e.g*., Koons and Fennel, 2006; Baker *et al*., 2017). For example, the Galaxy 15 satellite had its communication system partially shut down

due to electrostatic discharges caused by solar wind particles on 5 April 2010, turning it into a "zombie" satellite for the following 8 months (Horne *et al*., 2013). The company responsible for Galaxy 15 operations reported that the nearly fatal anomaly occurred around 09:48 UT (Allen, 2010), a period when Galaxy 15 drifted around geosynchronous locations. As estimated by Loto'aniu *et al*. (2015), the magnetopause standoff position during that period was within geosynchronous orbit leaving the satellite exposed to solar wind energetic particles, which partially contributed with the failure of Galaxy 15's electronic systems.

As such, our study quantitatively estimated the multiple magnitudes and time series of this solar-terrestrial storm for the source solar flare, SFEs, ICMEs, geomagnetic storms, equatorward boundary of the auroral oval, and cosmic-ray variability, indicating extreme cases even including the record values. This result provides a quantitative basis for future discussions on the terrestrial and social impacts of such rare but extreme solar-terrestrial storms.

Acknowledgment

We thank Ciaran D. Beggan, Eliot Eaton, and Eleanor Maume for providing BGS magnetogram data and advice on their interpretations, Kosuke Fukuda, Panayiota Chrysikopoulou, and Ioannis A. Daglis for their help for interpretation of the Greek newspapers, Toshihiko Iyemori for his advice on the interpretation of SJG data, Ian Richardson for helpful comments on the rigidity dependence of Forbush decreases, and Raysa Magalhães Rocha for her advice on the VSS data. HH thanks financial supports of JSPS Grant-in-Aids JP15H05812, JP18H01254, JP20K20918, and JP20H05643, JSPS Overseas Challenge Program for Young Researchers, the 2020 YLC collaborating research fund, and the research grants for Mission Research on Sustainable Humanosphere from Research Institute for Sustainable Humanosphere (RISH) of Kyoto University and the ISEE director's leadership fund for FY2021 and Young Leader Cultivation (YLC) program of Nagoya University. DMO acknowledges financial support provided by the NASA Space Weather Science Applicarions Operations 2 Research program (grant # 20-SWO2R20-2-0014). DRF thanks research funding agency FAPERJ for the grant # E-26/203.302/2017. SPB thanks NASA's Living With a Star program (17-LWS17_2-0042). AB thanks the DST-INSPIRE Faculty fellowship, Department Of Science &

Technology, Gov. of India. HH has been benefited from discussions within the ISSI International Team #510 (SEESUP Solar Extreme Events: Setting Up a Paradigm) and ISWAT-COSPAR S1-02 team. We thank Mt. Wilson Observatory for providing sunspot drawings on 23 March 1940, WDC for Geomagnetism at Edinburgh for providing geomagnetic baselines and British magnetograms, WDC for Geomagnetism at Kyoto for providing the Dst index and magnetic measurements at Hermanus, San Juan, Honolulu, and Watheroo, Kakioka Event Database for providing data on the SSC and magnetic storms observed in the said observatory, the Service of Rapid Magnetic Variations (SRMV) held by Ebro Observatory for elaborating and maintaining SFE and SSC lists, WDC SILSO for providing international sunspot numbers, and Solar Science Observatory of the NAOJ for providing copies of Quarterly Bulletin on Solar Activity. Magnetograms were digitised using the WebPlotDigitizer software (https://automeris.io/WebPlotDigitizer/).

Data Availability

We consulted Kakioka Event Database and the Service of Rapid Magnetic Variations (SRMV: Ebro Observatory) for the spot values of the SSCs and geomagnetic storms observed, the NCEI Database of the Solar Sunspot Regions for the contemporary sunspot active regions, the Mt. Wilson Observatory for the contemporary sunspot drawings, WDC for Geomagnetism at Edinburgh for geomagnetic baselines and scans and digitisations of British magnetograms, WDC for Geomagnetism at Kyoto for the Dst index and magnetic measurements at Hermanus, San Juan, Honolulu, and Watheroo, WDC SILSO for international sunspot numbers, and Solar Science Observatory of the NAOJ for copies of Quarterly Bulletin on Solar Activity.

References

Allen, J., Frank, L., Sauer, H., Reiff, P.: 1989, *Eos, Transactions American Geophysical Union*, **70**, 1479–1488. DOI: 10.1029/89EO00409

Allen, J.: 2010, *Space Weather*, **8**, 6. DOI:10.1029/2010SW000588

Araki, T., Keika, K., Kamei, T., Yang, H., Alex, S.: 2006, *Earth, Planets and Space*, **58**, 45-50. DOI: 10.1186/BF03351912

Araki, T.: 2014, *Earth, Planets and Space*, **66**, 164. DOI: 10.1186/s40623-014-0164-0

AN SSSR: 1954, *Astronomicheskii tsirkuliar (vol. 2)*, Akademiia nauk SSSR. Biuro astronomicheskikh soobshchenii. [in Russian]

Bailey, D. K.: 1964, *Planetary and Space Science*, **12**, 495-541. DOI: 10.1016/0032-0633(64)90040-6

Baker, D. N., Erickson, P. J., Fennell, J. F., Foster, J. C., Jaynes, A. N., Verronen, P. T.: 2017, *Space Science Reviews*, **24**, 17, 1-60. DOI: 10.1007/s11214-017-0452-7

Baker, D. N., *et al*.: 2008, *Severe space weather events—understanding societal and economic impacts*. National Academies Press, Washington DC

Balan, N., Zhang, Q.-H., Xing, Z., Skoug, R., Shiokawa, K., Lühr, H., Tulasi Ram, S., Otsuka, Y., Zhao, L.: 2019, *The Astrophysical Journal*, **887**, 51. DOI: 10.3847/1538-4357/ab5113

Balan, N., Tulasiram, S., Kamide, Y., Batista, I. S., Souza, J. R., Shiokawa, K., Rajesh, P. K., Victor, N. J.: 2017, *Earth, Planets and Space*, **69**, 59. DOI: 10.1186/s40623-017-0642-2

Baumjohann, W., Treumann, R.: 2009, *Basic Space Plasma Physics*, London, Imperial College Press.

Belov, A., Papaioannou, A., Abunina, M., Dumbovic, M., Richardson, I. G., Heber, B., Kuhl, P., Herbst, K., Anastasiadis, A., Vourlidas, A., Eroshenko, E., Abunin, A.: 2021, *The Astrophysical Journal*, **908**, 5. DOI: 10.3847/1538-4357/abd724

Besprozvannaya, A. S.: 1962, *Journal of the Physical Society of Japan*, **17**, Supplement A-I, 146-149.

Blake, S. P., *et al*., 2020, *Journal of Geophysical Research: Space Physics*, **125**, e27336. DOI: 10.1029/2019JA027336

Blake, S. P., Pulkkinen, A., Schuck, P. W., Glocer, A., Oliveira, D. M., Welling, D., Weigel, R. S., Quaresima, G.: 2021. *Space Weather*, **19**, e2020SW002585. DOI: 10.1029/2020SW002585

Bolduc, L.: 2002, *Journal of Atmospheric and Solar-Terrestrial Physics*, **64**, 1793-1802. DOI: 10.1016/S1364-6826(02)00128-1

Boteler, D. H.: 2001, Space weather effects on power systems, *Space Weather, Geophys. Monogr. Ser.*, vol. 125, edited by P. Song, H. J. Singer, and G. L. Siscoe, pp. 347-352, AGU, Washington, D. C. DOI: 10.1029/GM125p0347

Boteler, D. H.: 2019, *Space Weather*, **17**, 1427–1441. DOI: 10.1029/2019SW002278

Boteler, D. H., Pirjola, R. J.: 2014, *Annales Geophysicae*, **32**, 1177-1187. DOI: 10.5194/angeo-32-1177-2014

Burton, R. K., McPherron, R. L., Russell, C. T.: 1975, *Journal of Geophysical Research*, **80**, 4204–4214. DOI: 10.1029/JA080i031p04204

Clette, F., Lefèvre, L.: 2016, *Solar Physics*, **291**, 2629–2651. DOI: 10.1007/s11207-016-1014-y

Cliver, E. W., Dietrich, W. F.: 2013, *Journal of Space Weather and Space Climate*, **3**, A31. DOI: 10.1051/swsc/2013053

Cliver, E. W., Feynman, J., Garrett, H. B.: 1990, *Journal of Geophysical Research*, **95**, A10, 17103-17112. DOI: 10.1029/JA095iA10p17103

Cliver, E. W., Hayakawa, H., Love, J. J., Neidig, D. F.: 2020, *The Astrophysical Journal*, **903**, 41. DOI: 10.3847/1538-4357/abad93

Cliver, E. W., Svalgaard, L.: 2004, *Solar Physics*, **224**, 407-422. DOI: 10.1007/s11207-005-4980-z

Cliver, E., Svalgaard, L., Ling, A.: 2004, *Annales Geophysicae*, **22**, 93-100. DOI: 10.5194/angeo-22-93-2004

Cummings, W. D.: 1966, *Journal of Geophysical Research*, **71**, 4495-4503, DOI: 10.1029/JZ071i019p04495.

Curto, J. J., Cardús, J. O., Alberca, L. F., Blanch, E.: 2007, *Earth, Planets and Space*, **59**, 463–471. DOI: 10.1186/BF03352708

Curto, J. J., Castell, J., Del Moral, F.: 2016, *Journal of Space Weather and Space Climate*, **6**, A23. DOI: 10.1051/swsc/2016018

Curto, J. J.: 2020, *Journal of Space Weather and Space Climate*, **10**, 27. DOI: 10.1051/swsc/2020027

D'Azambuja, L.: 1940, *Quarterly Bulletin on Solar Activity*, Nos. 49, Zürich, Edigen. Sternwarte.

Da Gama, S.: 1944, *Boletim Magnetico do Observatrio Nacional, Rio de Janeiro, 1940 e 1941*, Rio de Janeiro, Imprensa Nacional.

Daglis, I. A., Thorne, R. M., Baumjohann, W., Orsini, S.: 1999, *Reviews of Geophysics*, **37**, 407–438. DOI: 10.1029/1999RG900009

Davidson, W. F.: 1940, *Edison Electric Institute Bulletin*, **1940-07**, 365–366 and 374.

Ebihara, Y., Ejiri, M., Nilsson, H., Sandahl, I., Milillo, A., Grande, M., Fennell, J. F., Roeder, J. L.: 2002, *Geophysical Research Letters*, **29**, 3031-3034, DOI:10.1029/2002GL015430

Ebihara, Y., Ejiri, M.: 2000, *Journal of Geophysical Research*, **105**, A7, 15843-15860. DOI: 10.1029/1999JA900493

Ebihara, Y., Fok, M. -C., Immel, T. J., Brandt, P. C.: 2011, *Journal of Geophysical Research: Space Physics*, **116**, A3, A03218. DOI: 10.1029/2010ja016000

Ebihara, Y., Hayakawa, H., Iwahashi, K., Tamazawa, H., Kawamura, A. D., Isobe, H.: 2017, *Space Weather*, **15**, 1373–1382. DOI: 10.1002/2017SW001693

Ellison, M. A.: 1940, *Nature*, **145**, 898. DOI: 10.1038/145898b0

Flammarion, G. C., Quenisset, F.: 1940, *L'Astronomie*, **54**, 88-89

Freed, A. J., Russell, C. T.: 2014, *Geophysical Research Letters*, **41**, 6590-6594. DOI: 10.1002/2014GL061353

Germaine, L. W.: 1940, *Edison Electric Institute Bulletin*, **1940-07**, 367

Gonzalez, W. D., Echer, E., Tsurutani, B. T., Clúa de Gonzalez, A. L., Dal Lago, A.: 2011, *Space Science Reviews*, **158**, 69-89. DOI: 10.1007/s11214-010-9715-2

Gonzalez, W. D., Joselyn, J. A., Kamide, Y., Kroehl, H. W., Rostoker, G., Tsurutani, B. T., Vasyliunas, V. M.: 1994, *Journal of Geophysical Research*, **99**, A4, 5771-5792. DOI: 10.1029/93JA02867

Gopalswamy, N., Yashiro, S., Liu, Y., Michalek, G., Vourlidas, A., Kaiser, M. L., Howard, R. A.: 2005, *Journal of Geophysical Research: Space Physics*, **110**, A9, A09S15. DOI: 10.1029/2004JA010958

Hamilton, D. C., Gloeckler, G., Ipavich, F. M., Stüdemann, W., Wilken, B., Kremser, G.: 1986, *Journal of Geophysical Research*, **93**, A12, 14343-14355. DOI: 10.1029/JA093iA12p14343

Hapgood, M.: 2017, Linking space weather science to impacts — The view from Earth. In N. Buzulukova (ed.), *Extreme Space Weather: Origins, Predictability, and Consequences*, pp. 3 – 34, Amsterdam, Elsevier.

Hapgood, M., Angling, M. J., Attrill, G., *et al.*: 2021, *Space Weather*, **19**, e02593. DOI: 10.1029/2020SW002593

Hathaway, D. H.: 2015, *Living Reviews in Solar Physics*, **12**, 4. DOI: 10.1007/lrsp-2015-4

Hayakawa, H., Blake, S. P., Bhaskar, A., Hattori, K., Oliveira, D. M., Ebihara, Y.: 2021a, *The Astrophysical Journal*. DOI: 10.3847/1538-4357/abb772

Hayakawa, H., Ebihara, Y., Cliver, E. W., *et al*., 2019a, *Monthly Notices of the Royal Astronomical Society*, **484**, 4083-4099. DOI: 10.1093/mnras/sty3196

Hayakawa, H., Ebihara, Y., Hata, H.: 2022, *Geoscience Data Journal*, DOI: 10.1002/GDJ3.140

Hayakawa, H., Ebihara, Y., Willis, D. M., *et al*.: 2018, *The Astrophysical Journal*, **862**, 15. DOI: 10.3847/1538-4357/aaca40

Hayakawa, H., Ebihara, Y., Willis, D. M., *et al*.: 2019b, *Space Weather*, **17**, 1553–1569. DOI: 10.1029/2019SW002269

Hayakawa, H., Ebihara. Y., Pevtsov, A. A., Bhaskar, A., Karachik, N., Oliveira, D. M.: 2020b, *Monthly Notices of the Royal Astronomical Society*, **497**, 5507-5517. DOI: 10.1093/mnras/staa1508

Hayakawa, H., Hattori, K., Pevtsov, A. A., *et al*.: 2021b, *The Astrophysical Journal*, DOI: 10.3847/1538-4357/abc427

Hayakawa, H., Nevanlinna, H., Blake, S. P., Ebihara, Y., Bhaskar, A. T., Miyoshi, Y.: 2021c, *The Astrophysical Journal*, DOI: 10.3847/1538-4357/ac2601

Hayakawa, H., Ribeiro, J. R., Ebihara, Y., Correira, A. P., Soma, M.: 2020c, *Earth, Planets and Space*, **72**, 122. DOI: 10.1186/s40623-020-01249-4

Hayakawa, H., Ribeiro, P., Vaquero, J. M., *et al*.: 2020a, *The Astrophysical Journal Letters*, **897**, L10. DOI: 10.3847/2041-8213/ab6a18

Hershberger, J.: 1940, *Terrestrial Magnetism and Atmospheric Electricity*, **45**, 228-228. DOI: 10.1029/TE045i002p00228

Hoffman, R. A., Cahill, L. J., Anderson, R. R., Maynard, N. C., Smith, P. H., Fritz, T. A., Williams, D. J, Konradi, A., Gurnett, D. A.: 1975, *Journal of Geophysical Research*, **80**, 4287-4296, DOI: 10.1029/JA080i031p04287

Horne, R. B., Glauert, S. A., Meredith, N. P., Boscher, D., Maget, V., Heynderickx, D., Pitchford, D.: 2013, *Space Weather*, **11**, 4, 169–186. DOI:10.1002/swe.20023

Huba, J. D., Sazykin, S.: 2014, *Geophysical Research Letters*, **41**, 8208-8214. DOI: 10.1002/2014GL062110

Jones, H. S.: 1953, *Results of the magnetic and meteorological observations made at the Abinger magnetic station, surrey and the Royal Observatory, Greenwich respectively in the year 1940*, London: Her Majesty's Stationery Office

Jones, H. S.: 1955, *Sunspot and geomagnetic-storm data derived from Greenwich observations, 1874-1954: derived from Greenwich Observations, 1874-1954*, London, Her Majesty's Stationery Office.

Karoff, C., Knudsen, M. F., De Cat, P., *et al*.: 2016, *Nature Communications*, **7**, 11058. DOI: 10.1038/ncomms11058

Karinen, A., Mursula, K.: 2005, *Annales Geophysicae*, **23**, 475–485.

Kilpua, E. K. J., Olspert, N., Grigorievskiy, A., *et al*.: 2015, *The Astrophysical Journal*, **806**, 272. DOI: 10.1088/0004-637X/806/2/272

Knipp, D. J., Bernstein, V., Wahl, K., Hayakawa, H.: 2021, *Journal of Space Weather and Space Climate*, **11**, 29. DOI: 10.1051/swsc/2021011

Knipp, D. J., Fraser, B. J., Shea, M. A., Smart, D. F.: 2018, *Space Weather*, **16**, 1635-1643. DOI: 10.1029/2018SW002024

Knipp, D. J., Ramsay, A. C., Beard, E. D., *et al*.: 2016, *Space Weather*, **14**, 614-633. DOI: 10.1002/2016SW001423

Koons, H. C., Fennell, J. F.: 2006. *The Radio Science Bulletin*, **2006**, 27-41. DOI:10.23919/URSIRSB.2006.7909358

Kozyra, J. U., Fok, M. -C., Sanchez, E. R., Evans, D. S., Hamilton, D. C., Nagy, A. F.: 1998, *Journal of Geophysical Research*, **103**, A4, 6801-6814. DOI: 10.1029/97JA03330

Lakhina, G. S., Tsurutani, B. T.: 2016, *Geoscience Letters*, **3**, 1–11. DOI:10.1186/s40562-016- 0037-4

Lakhina, G. S., Tsurutani, B. T.: 2017, Supergeomagnetic storms: Past, present, and future. In N. Buzulukova (ed.), *Extreme Space Weather: Origins, Predictability, and Consequences*, pp. 157– 186, Amsterdam, Elsevier.

Lange, I., Forbush, S. E.: 1948, *Research of the Department of Terrestrial Magnetism, XIV*, Washington DC, Carnegie Institute of Washington Publication.

Lange, I., Forbush, S. E.: 1957, *Research of the Department of Terrestrial Magnetism, XX*, Washington DC, Carnegie Institute of Washington Publication.

Lanzerotti, L. J.: 2017, *Space Science Reviews*, **212**, 1253-1270. DOI: 10.1007/s11214-017-0408-y

Le, H., Liu, L., He, H., Wan, W.: 2011, *Journal of Geophysical Research*, **116**, A11301. DOI: 10.1029/2011JA016704

Lefèvre, L., Vennerstrøm, S., Dumbović, M., Vršnak, B., Sudar, D., Arlt, R., Clette, F., Crosby, N.: 2016, *Solar Physics*, **291**, 1483–1531. DOI: 10.1007/s11207-016-0892-3

Liu, Y. D., Luhmann, J. G., Kajdic, P., Kilpua, E. K. J., Lugaz, N., Nitta, N. V., Moestl, C., Lavraud, B., Bale, S. D., Farrugia, C. J., Galvin, A. B.: 2014, *Nature Communications*, **5**, 3481. DOI:10.1038/ncomms4481

Liu, Y. D., Zhao, X., Hu, H., Vourlidas, A., Zhu, B.: 2019, *The Astrophysical Journal Supplement Series*, **241**, 15. DOI: 10.3847/1538-4365/ab0649

Lockwood, M., Chambodut, A., Barnard, L. A., Owens, M. J., Clarke, E., Mendel, V.: 2018a, *Journal of Space Weather and Space Climate*, **8**, A53. DOI: 10.1051/swsc/2018038

Lockwood, M., Finch, I. D., Chambodut, A., Barnard, L. A., Owens, M. J., Clarke, E.: 2018b, *Journal of Space Weather and Space Climate*, **8**, A58. DOI: 10.1051/swsc/2018044

Loto'aniu, T. M., Singer, H. J., Rodriguez, J. V., Green, J., Denig, W., Biesecker, D., Angelopoulos, V.: 2015, *Space Weather*, **13**, 484-502. DOI:10.1002/2015SW001239

Love, J. J., Hayakawa, H., Cliver, E. W.: 2019a, *Space Weather*, **17**, 37-45. DOI: 10.1029/2018SW002079

Love, J. J., Hayakawa, H., Cliver, E. W.: 2019b, *Space Weather*, **17**, 1281–1292. DOI: 10.1029/2019SW002250

Love, J. J.: 2018, *Space Weather*, **16**, 37-46. DOI: 10.1002/2017SW001795

Löwe, C. A., Prölss, G. W.: 1997, *Journal of Geophysical Research*, **102**, A7, 14209–14213, DOI: 10.1029/96JA04020

Mannucci, A. J., Tsurutani, B. T., Iijima, B. A., *et al*.: 2005, *Geophysical Research Letters*, **32**, L12S02. DOI: 10.1029/2004GL021467

McCracken, K .G.: 2007, *Space Weather*, **5**, 07004. DOI: 10.1029/2006SW000295

McIntosh, D. H.: 1951, *Journal of Atmospheric and Terrestrial Physics*, **1**, 315-342. DOI: 10.1016/0021-9169(51)90006-2

McNish, A. G.: 1940, *Terrestrial Magnetism and Atmospheric Electricity*, **45**, 359-364. DOI: 10.1029/TE045i003p00359

Meng, X., Tsurutani, B. T., Mannucci, A. J.: 2019, *Journal of Geophysical Research: Space Physics*, **124**, 3926–3948, DOI: 10.1029/2018JA026425

Miyake, F., Usoskin, I. G., Poluianov, S.: 2019, *Extreme Solar Particle Storms: The hostile Sun*, Bristol, IOP. DOI: 10.1088/2514-3433/ab404a

Mursula, K., Holappa, L., Karinen, A.: 2008, *Astrophys. Space Sci. Trans. (ASTRA)*, **4**, 41. DOI: 10.5194/astra-4-41-2008

Newton, H. W.: 1940, *The Observatory*, **63**, 129-134

Nicholson, S. B.: 1940, *Publications of the Astronomical Society of the Pacific*, **52**, 169-171. DOI: 10.1086/125156

Notsu, Y., Maehara, H., Honda, S., *et al*.: 2019, *The Astrophysical Journal*, **876**, 58. DOI: 10.3847/1538-4357/ab14e6

Ogg, A.: 1941, *Terrestrial Magnetism and Atmospheric Electricity*, **46**, 118-120. DOI: 10.1029/TE046i001p00118-02

Oliveira, D. M., Arel, D., Raeder, J., Zesta, E., Ngwira, C. M., Carter, B. A., Yizengaw, E., Halford, A. J., Tsurutani, B. T., Gjerloev, J. W.: 2018, *Space Weather*, **16**, 636-647. DOI: 10.1029/2018SW001880

Oliveira, D. M., Hartinger, M. D., Xu, Z., Zesta, E., Pilipenko, V. A., Giles, B. L., & Silveira, M. V. D.: 2020b, *Geophysical Research Letters*, **47**, e2020GL090857. DOI: 10.1029/2020GL090857

Oliveira, D. M., Samsonov, A. A.: 2018, *Advances in Space Research*, **61**, 1-44. DOI: 10.1016/j.asr.2017.10.006

Oliveira, D. M., Zesta, E., Hayakawa, H., Bhaskar, A. T.: 2020a, *Space Weather*, **18**, e2020SW002472. DOI: 10.1029/2020SW002472

Oliveira, D. M., Zesta, E., Mehta, P. M., Licata, R. J., Pilinski, M. D., Tobiska, W. K., Hayakawa, H. 2021a, *Frontiers in Astronomy and Space Science*, **8**, 764144. DOI: 10.3389/fspas.2021.764144

Oliveira, D. M., Weygand, J. M., Zesta, E., Ngwira, C. M., Hartinger, M. D., Xu, Z., Giles, B. L., Gershman, D. J., Reeves, G. D., Silveira, M. V. D., Souza, V. M.: 2021b, *Space Weather*, DOI: 10.1029/2021SW002933

Oughton, E. J., Skelton, A., Horne, R. B., Thomson, A. W. P., Gaunt, C. T.: 2017, *Space Weather*, **15**, 65-83. DOI: 10.1002/2016SW001491

Parkinson, W. C.: 1940, *Terrestrial Magnetism and Atmospheric Electricity*, **45**, 233-234. DOI: 10.1029/TE045i002p00233

Pevtsov, A. A., Tlatova, K. A., Pevtsov, A. A., Heikkinen, E., Virtanen, I., Karachik, N. V., Bertello, L., Tlatov, A. G., Ulrich, R., Mursula, K.: 2019a, *Astronomy & Astrophysics*, **628**, A103. DOI: 10.1051/0004-6361/201834985

Pevtsov, A., Griffin, E., Grindlay, J., *et al*.: 2019b, *Bulletin of the American Astronomical Society*, **51**, 190.

Plakidis, F., Anastasiadis, M. A., Chrysanthis, A.: 1940, *ΠΡΑΚΤΙΚΑ ΤΗΣ ΑΚΑΔΗΜΙΑΣ ΑΘΗΝΩΝ*, **15**, 417-421.

Pulkkinen, A., Bernabeu, E., Thomson, A., *et al*., 2017, *Space Weather*, **15**, 828-856. DOI: 10.1002/2016SW001501

Pulkkinen, A., Lindahl, S., Viljanen, A., Pirjola, R.: 2005, *Space Weather*, **3**, S08C03. DOI: 10.1029/2004SW000123

Pulkkinen, T.: 2007, *Living Reviews in Solar Physics*, **4**, 1. DOI: 10.12942/lrsp-2007-1

Raghav, A. N., Choraghe, K., Shaikh, Z. I.: 2019, *Monthly Notices of the Royal Astronomical Society*, **488**, 910–917. DOI: 10.1093/mnras/stz1608

Raghav, A. N., Kule, A., Bhaskar, A., Mishra, W., Vichare, G., Surve, S.: 2018, *The Astrophysical Journal*, **860**, 26.

Rangaswami, M. R.: 1940, *Terrestrial Magnetism and Atmospheric Electricity*, **45**, 382-383. DOI: 10.1029/TE045i003p00382

Ravishankar, A., Michałek, G.: 2019, *Solar Physics*, **294**, 125. DOI: 10.1007/s11207-019-1470-2

Richardson, I. G., Cane, H.V., 2011, *Solar Physics*, **270**, 609-627. DOI: 10.1007/s11207-011-9774-x

Riley, P., Baker, D., Liu, Y. D., Verronen, P., Singer, H., Güdel, M.: 2018, *Space Science Reviews*, **214**, 21. DOI: 10.1007/s11214-017-0456-3

Riley, P.: 2017, Statistics of Extreme Space Weather Events, in: N. Buzulukova (ed.), *Extreme Events in Geospace: Origins, Predictability, and Consequences*, pp. 115 – 138, Amsterdam, Elsevier.

Roach, F. E., Moore, J. G., Bruner, E. C., Jr., Cronin, H., Silverman, S. M.: 1960, *Journal of Geophysical Research*, **65**, 3575–3580. DOI: 10.1029/JZ065i011p03575

Rudd, J. T., Oliveira, D. M., Bhaskar, A., Halford, A. J.: 2019, *Advances in Space Research*, **63**, 317-326. DOI: 10.1016/j.asr.2018.09.013

Russell, C. T., McPherron, R. L.: 1973, *Journal of Geophysical Research*, **78**, 92-108. DOI: 10.1029/JA078i001p00092

Schrijver, C. J.: 2015, *Space Weather*, **13**, 524-528. DOI: 10.1002/2015SW001252

Sellers, B., Hanser, F. A., Stroscio, M. A., Yates, G. K.: 1977, *Radio Sci.*, **12**, 779-789.

Shea, M. A., Smart, D. F.: 1990, *Solar Physics*, **127**, 297-320. DOI: 10.1007/BF00152170

Shea, M. A., Smart, D. F.: 2000, *Space Science Reviews*, **93**, 229-262. DOI: 10.1023/A:1026500713452

Shea, M. A., Smart, D. F.: 2012, *Space Science Reviews*, **171**, 161-188. DOI: 10.1007/s11214-012-9923-z

Shea, M. A., Smart, D. F.: 2019, *International Cosmic Ray Conference (ICRC2019, Madison)*, **36**, 1149.

Shiokawa, K., Yumoto, K., Tanaka, Y., Oguti, T., Kiyama, Y.: 1994, *Journal of Geomagnetism and Geoelectricity*, **46**, 231-252. DOI: 10.5636/jgg.46.231

Shiota, D., Kataoka, R.: 2016, *Space Weather*, **14**, 56-75. DOI: 10.1002/2015SW001308

Shue, J. -H., Song, P., Russell, C. T., *et al*.: 1998, *Journal of Geophysical Research*, **103**, A8, 17691-17700. DOI: 10.1029/98JA01103

Silverman, S. M., Cliver, E. W.: 2001, *Journal of Atmospheric and Solar-Terrestrial Physics*, **63**, 523-535. DOI: 10.1016/S1364-6826(00)00174-7

Silverman, S. M.: 2006, *Advances in Space Research*, **38**, 136-144. DOI: 10.1016/j.asr.2005.03.157

Siscoe, G. L., Formisano, V., Lazarus, A. J.: 1968, *Journal of Geophysical Research*, **73**, 4869–4874. DOI: 10.1029/JA073i015p04869

Siscoe, G., Crooker, N. U., Clauer, C. R.: 2006, *Advances in Space Research*, **38**, 173–179. DOI: 10.1016/j.asr.2005.02.102

Smart, D. F., Shea, M. A.: 1979, PPS76 - A Computerized "Event Mode" Solar Proton Forecasting Technique, *Solar-Terrestrial Predictions Proceedings*, Volume 1: Prediction Group Reports, Edited by Richard F. Donnelly, Environment Research Laboratories, National Oceanic and Atmospheric Administration, U.S. Department of Commerce, Boulder, Colorado, 406-427.

Stanislawska, I., Gulyaeva, T. L., Grynyshyna-Poliuga, O., Pustovalova, L. V.: 2018, *Space Weather*, **16**, 2068-2078. DOI: 10.1029/2018SW001945

Sugiura, M., Kamei, T.: 1999, *IAGA Bull*. **40**, IUGG, Paris.

Sugiura, M.: 1964, *Ann. Int. Geophys. Year*, **35**, 9–45, Oxford, Pergamon Press.

Suiro Yoran: 1940, *Suiro Yoran*, **211**, 219. [in Japanese]

Svalgaard, L.: 2011, *Geophysical Research Letters*, **38**, L16107. DOI: 10.1029/2011GL048616

Švestka, Z.: 1966, *Space Science Reviews*, **5**, 388–418. DOI: 10.1007/bf02653250

Švestka, Z. 1976, *Solar Flares*, Springer-Verlag, Berlin.

Thébault, E., Finlay, C. C., Beggan, C., *et al*.: 2015, *Earth, Planets and Space*, **67**, 79. DOI: 10.1186/s40623-015-0228-9

Thomson, A. W. P., McKay, A. J., Clarke, E., Reay, S. J.: 2005, *Space Weather*, **3**, S11002. DOI: 10.1029/2005SW000156

Tsurutani, B. T., & Lakhina, G. S.: 2014, *Geophysical Research Letters*, **41**, 287-292. DOI: 10.1002/2013GL058825

Tsurutani, B. T., Gonzalez, W. D., Lakhina, G. S., Alex, S.: 2003, *Journal of Geophysical Research Space Physics*, **108**, A7, 1268. DOI 10.1029/2002JA009504

Usoskin, I. G., Bazilevskaya, G. A., Kovaltsov, G. A.: 2011, *Journal of Geophysical Research*, **116**, A2, A02104. DOI: 10.1029/2010JA016105

Vaisberg, O. L., Zastenker, G. N.: 1976, *Space Science Reviews*, **19**, 687-702. DOI: 10.1007/BF00210646

Vichare, G., Rawat, R., Bhaskar, A., Pathan, B. M.: 2014, *Earth, Planets and Space*, **66**, 1-21. DOI: 10.1186/1880-5981-66-92

WDC for Geomagnetism at Kyoto, Nose, M., Iyemori, T., Sugiura, M., Kamei, T.: 2015, *Geomagnetic Dst Index*, DOI:10.17593/14515-74000

Welling, D. T., Love, J. J., Joshua Rigler, E., Oliveira, D. M., Komar, C. M., Morley, S. K.: 2021, *Space Weather*, **19**, e2020SW002489. DOI: 10.1029/2020SW002489

Wells, H. W.: 1940, *Terrestrial Magnetism and Atmospheric Electricity*, **45**, 381-381. DOI: 10.1029/TE045i003p00381-01

Wu, C.-C., Liou, K., Lepping, R. P., Hutting, L.: 2019, *Solar Physics*, **294**, 110. DOI:10.1007/s11207-019-1446-2

Xu, Z., Hartinger, M. D., Oliveira, D. M., Coyle, S., Clauer, C. R., Weimer, D., Edwards, T.: 2020, *Space Weather*, **18**, e2019SW002427. DOI: 10.1029/2019SW002427

Yokouchi, Y.: 1953, *Memoirs of the Kakioka Magnetic Observatory*, **13**, 191-203.

Yokoyama, N., Kamide, Y., Miyaoka, H.: 1998, *Annales Geophysicae*, **16**, 566-573. DOI: 10.1007/s00585-998-0566-z